Polychromatic beam reflectometer using an energy-dependent neutron detector

C.F. Majkrzak[1], N. C. Maliszewskyj[1], A. Osovizky[1,2], Y. Yehuda-Zada[3,4], J. Ziegler[1], K. Pritchard[1], N. Hadad[1], J. Cook[1], E. Binkley[1], P. Tsai[1], and F. Heinrich[1]

[1] NIST Center for Neutron Research, Gaithersburg, Maryland
[2] Rotem Industries Ltd., Rotem Industrial Park, Israel
[3] Ben Gurion University of the Negev, Beer Sheva, Israel
[4] Electronics & Control Laboratories, Nuclear Research Center- Negev, Beer-Sheva, Israel

We describe progress in the development of an energy-dependent neutron detector intended primarily for use in a polychromatic beam reflectometer CANDOR (for Chromatic Analyser Neutron Reflectometer Or Diffractometer) being constructed at the NIST Center for Neutron Research. The general design is applicable to other instruments as well, for example, a materials diffactometer (Simmons et al. *J. Appl. Cryst.* **46**, 2013). This detector incorporates pyrolytic graphite analyser crystals (54 separate elements in series) in conjunction with 6LiF/ZnS(Ag) scintillation detectors and silicon photomultiplier (SiPM) devices to form a module which simultaneously detects neutrons within a 4 to 6 Angstrom bandwidth with a fractional wavelength resolution of approximately one percent. Photons are produced by the interaction of the alpha and triton particles, originating from neutron capture in the Li, with the ZnS(Ag). Some fraction of these photons is subsequently channeled up through embedded wavelength-shifting fibers to the SiPM devices which produce, in turn, electrical pulses. Currently, neutron capture events are distinguished from gammas and background by pulse-width rather than pulse-height analysis (the gamma sensitivity is about seven orders of magnitude lower than that for neutrons). The sensitivity for neutron detection is dependent on light output intensity and neutron capture probability. The neutron detection efficiency of the scintillation detectors is currently limited to approximately 50 per cent (for a 1 mm thick slab that has an absorption of about 90 percent for 5 Angstrom neutron wavelengths) because the grain sizes of the 6LiF and ZnS(Ag) particles (in a polymer binder) are significantly larger than optimal (which is believed to be in the 2 to 4 micron range). It is expected that with the use of smaller grain sizes the efficiency will be significantly improved. How 30 such energy-dependent detector modules are to be configured into an array within the reflectometer is described, particularly in regard to achieving a focusing condition in the wavevector transfer Q for specular reflectivity measurements. For non-specular reflectivity measurements, an order of magnitude gain over a conventional monochromatic beam instrument at a continuous source is in principle possible, whereas for specular reflectivity measurements -- in which a broader angular divergence of the incident polychromatic beam can be used in addition -- a gain of several orders of magnitude may be realized under certain conditions.

We would also like to acknowledge the significant contributions from Brian Maranville and Dongwon Lee (NIST staff) in earlier stages of the project as well as discussions with members of the detector group at ISIS.

For a reflectometer/diffractometer at a pulsed neutron source, a substantial part of the entire wavelength distribution contained in a single pulse can be used to measure the reflectivity at multiple corresponding Q values by taking advantage of the intrinsic time structure, i.e., by labelling Q as a function of time of flight (Q is inversely proportional to the wavelength).

To be as efficient at a continuous source, another method for identifying different wavelengths present in a polychromatic beam is needed.

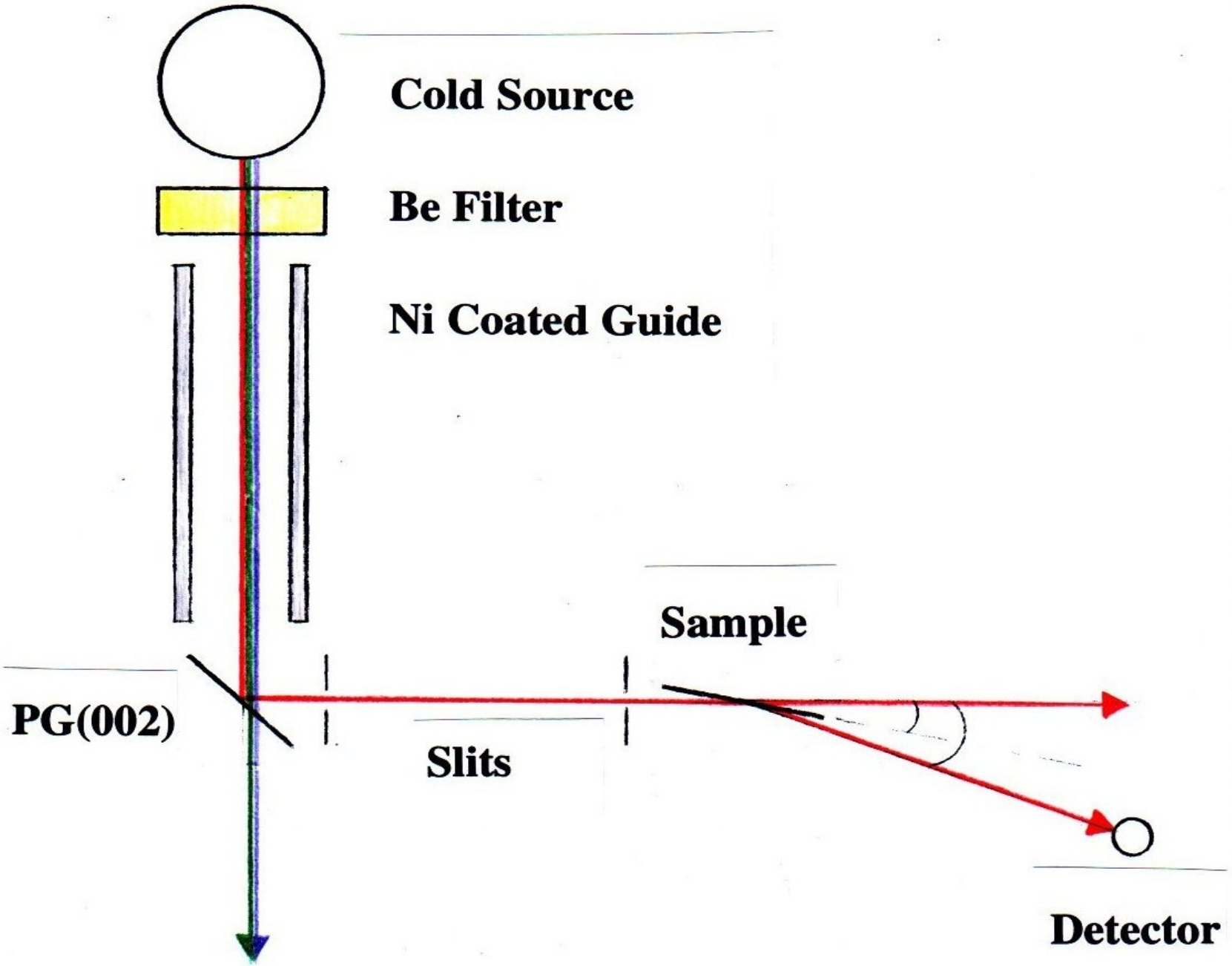
Cold Source
Be Filter
Ni Coated Guide
Sample
PG(002)
Slits
Detector

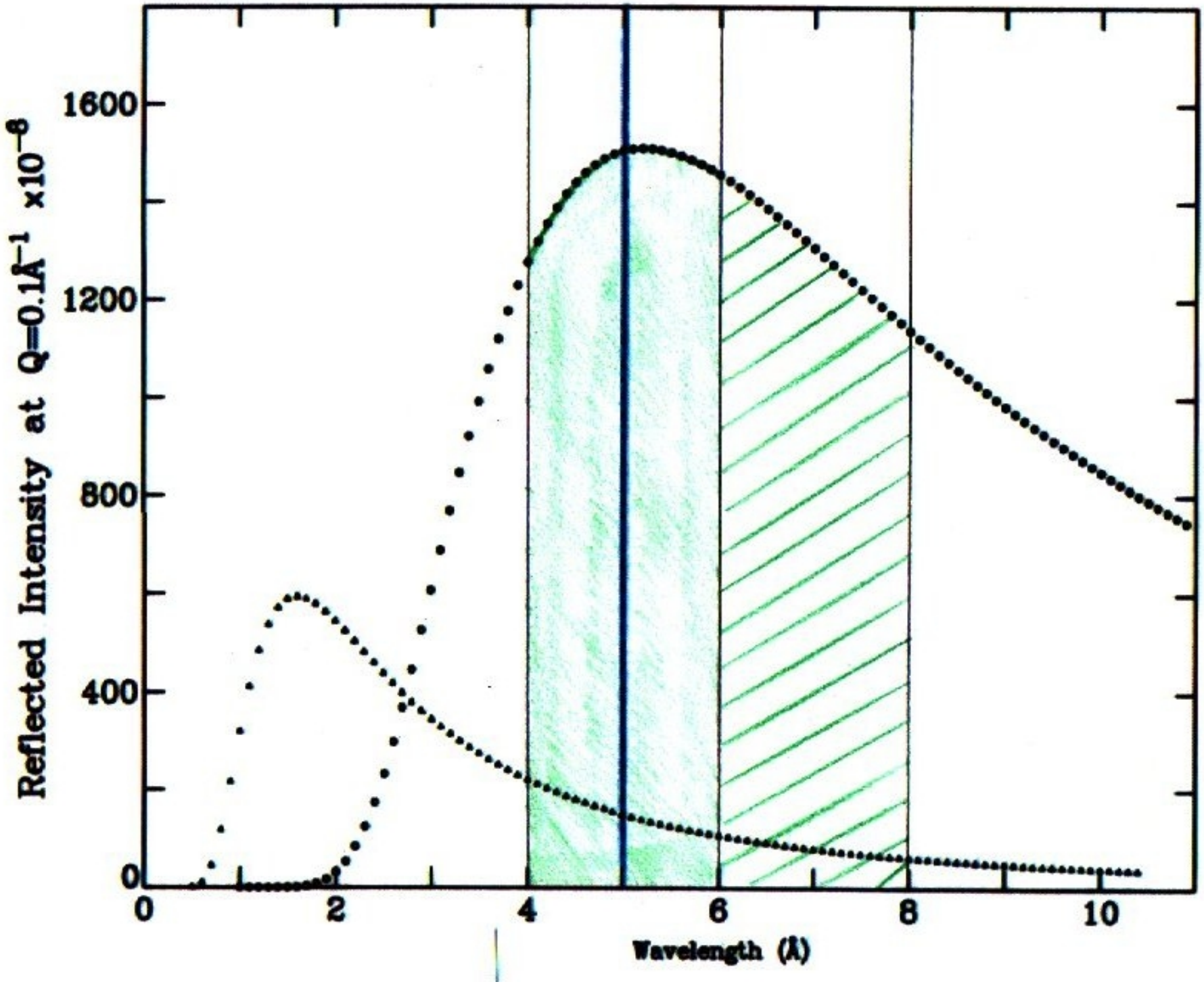
Reflected Intensity at Q=0.1Å^{-1} x10^{-6}
1600
1200
800
400
0
0
2
4
6
8
10
Wavelength (Å)

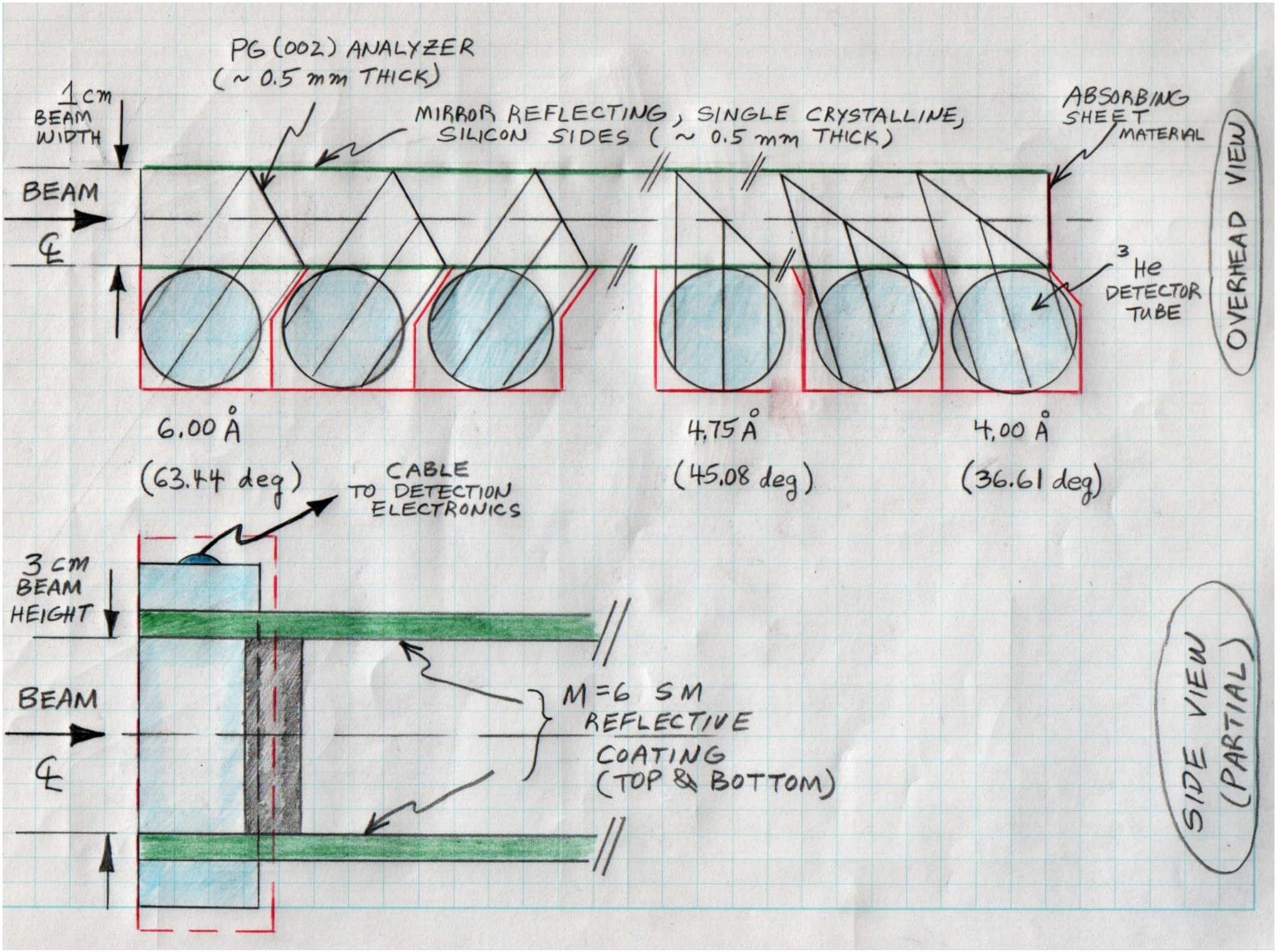
PG (002) ANALYZER
(~ 0.5 mm THICK)
1 cm
BEAM
WIDTH
MIRROR REFLECTING, SINGLE CRYSTALLINE,
SILICON SIDES (~ 0.5 mm THICK)
ABSORBING
SHEET
MATERIAL
BEAM
℄
^{3}He
DETECTOR
TUBE
OVERHEAD VIEW
6.00 Å
(63.44 deg)
4.75 Å
(45.08 deg)
4.00 Å
(36.61 deg)
CABLE
TO DETECTION
ELECTRONICS
3 cm
BEAM
HEIGHT
BEAM
℄
M=6 SM
REFLECTIVE
COATING
(TOP & BOTTOM)
SIDE VIEW
(PARTIAL)

Energy Dispersive Neutron Detectors for Steady-State Sources

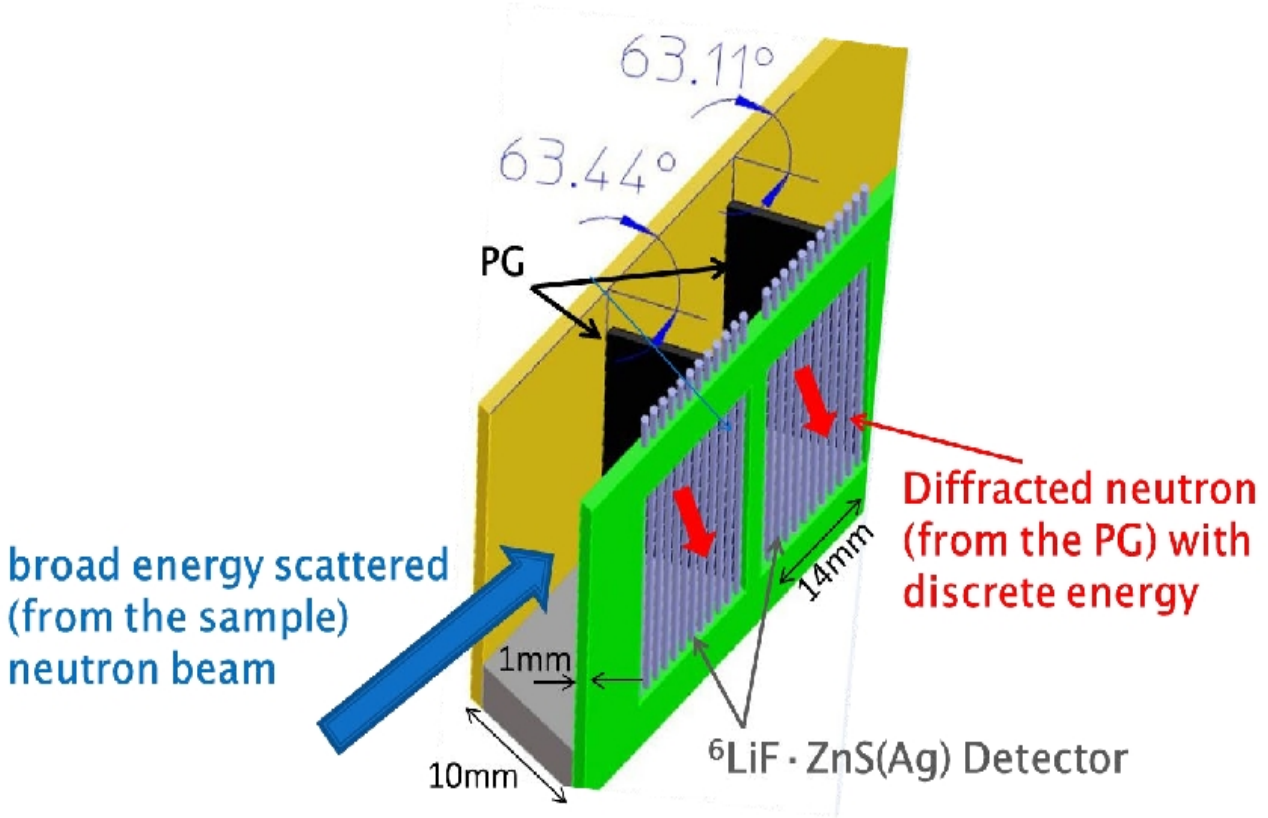

CANDoR

30 detection blocks

54 detectors/array

1620 detectors total

FY12 IMS

(Thanks to Rob Dimeo for this slide.)

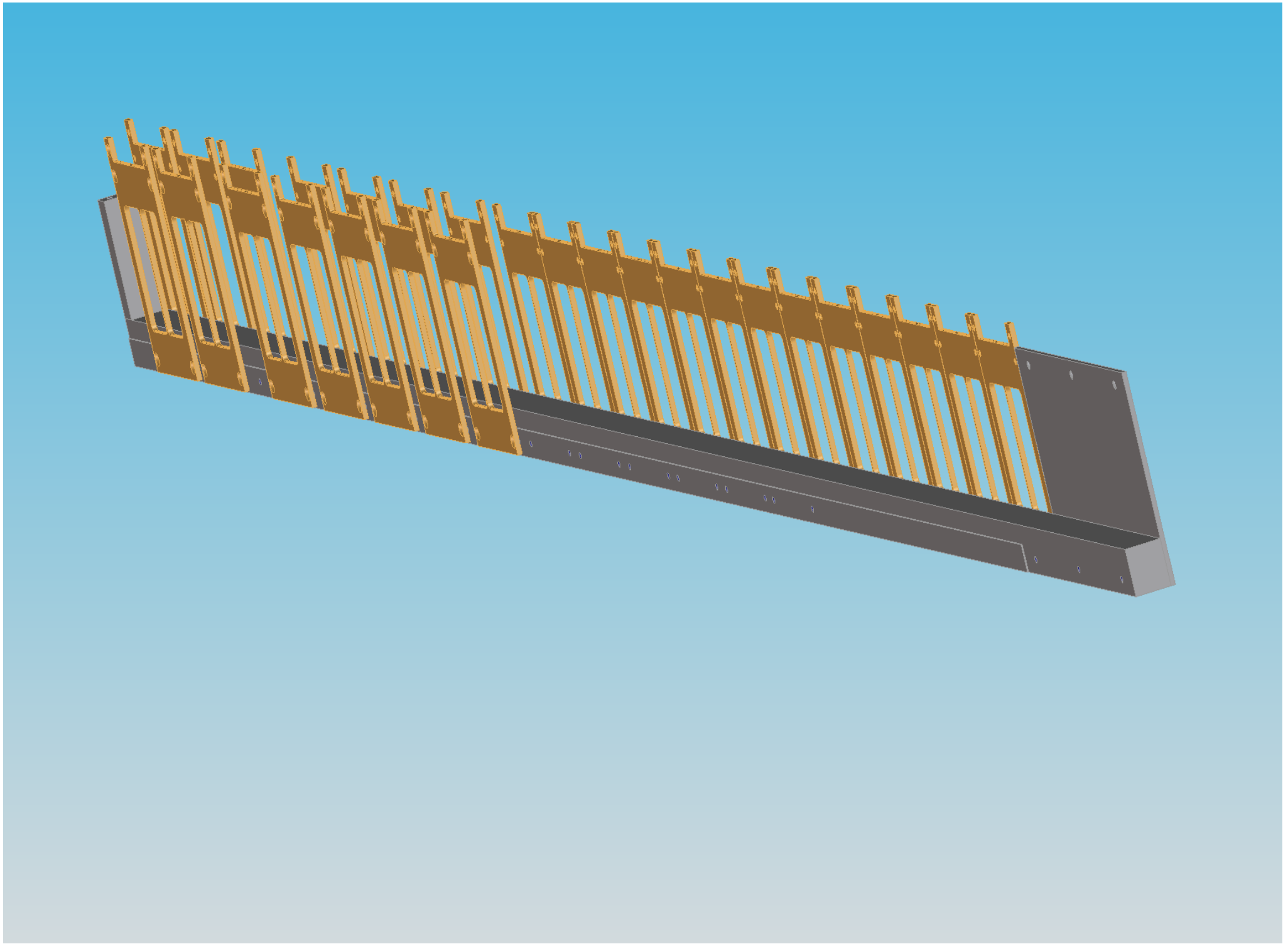

Journal of Neutron Research, 1994, Vol. 2, No. 1, pp. 1-19
Reprints available directly from the publisher
Photocopying permitted by license only

Printed in Malaysia

Neutron Reflectometry as Optical Imaging

W.A. HAMILTON[1], JOHN B. HAYTER[1] and G.S. SMITH[2]

1. Solid State Division, Oak Ridge National Laboratory, Oak Ridge, TN 37831
2. Manuel Lujan, Jr. Neutron Scattering Center, Los Alamos National Laboratory, Los Alamos, NM 87545

In this paper we show how a specularly reflecting mirror sample at grazing incidence may be treated as a simple imaging element, akin to a slit camera. An analysis of the imaging properties leads to a new and efficient means of measuring neutron reflectivity. The resolution of a reflectivity curve obtained by this scheme depends only on the geometry of the sample-to-detector arrangement, and is largely independent of incident beam collimation. In the absence of significant off-specular scattering, this method of data reduction allows a neutron reflectometer equipped with a linear position sensitive detector to use the higher intensity of a loosely collimated beam while achieving excellent resolution. To illustrate the principle, we present raw and reduced reflection data taken on the first runs of the newly commissioned neutron reflectometer at the High-Flux Isotope Reactor (HFIR) at the Oak Ridge National Laboratory (ORNL).

INTRODUCTION

In the last decade, measurement of the reflection of neutrons has become recognized as an effective probe of surface and interface structures ranging from just a few atoms to thick macromolecular multilayers [1,2,3,4,5]. Neutron reflectometry, and the complementary technique of X-ray reflectometry, have been used in studies of a diverse variety of surface structures, including: thin-film superconductors [6,7], soap films [8], polymer interfaces and multilayers [9,10] and model biological lipid membranes [11,12]. As in small-angle scattering and diffraction, the neutron technique offers certain advantages over its X-ray counterpart; manipulation of isotopic contrast to highlight specific regions of interest within a larger structure without altering the chemistry, and high sensitivity to magnetic structures.

The specular reflection coefficient for neutrons is an optical transform in the scattering vector of the neutron scattering length density profile. At high Q and low reflectivities this transform is given by the Rayleigh approximation [13,14],

$$R[Q] \approx \frac{(4\pi)^2}{Q^4}\left|\int_{-\infty}^{\infty}\frac{d\beta}{dz}e^{-iQz}dz\right|^2$$

Chromatic Analysis Neutron Diffractometer Or Reflectometer

CANDOR

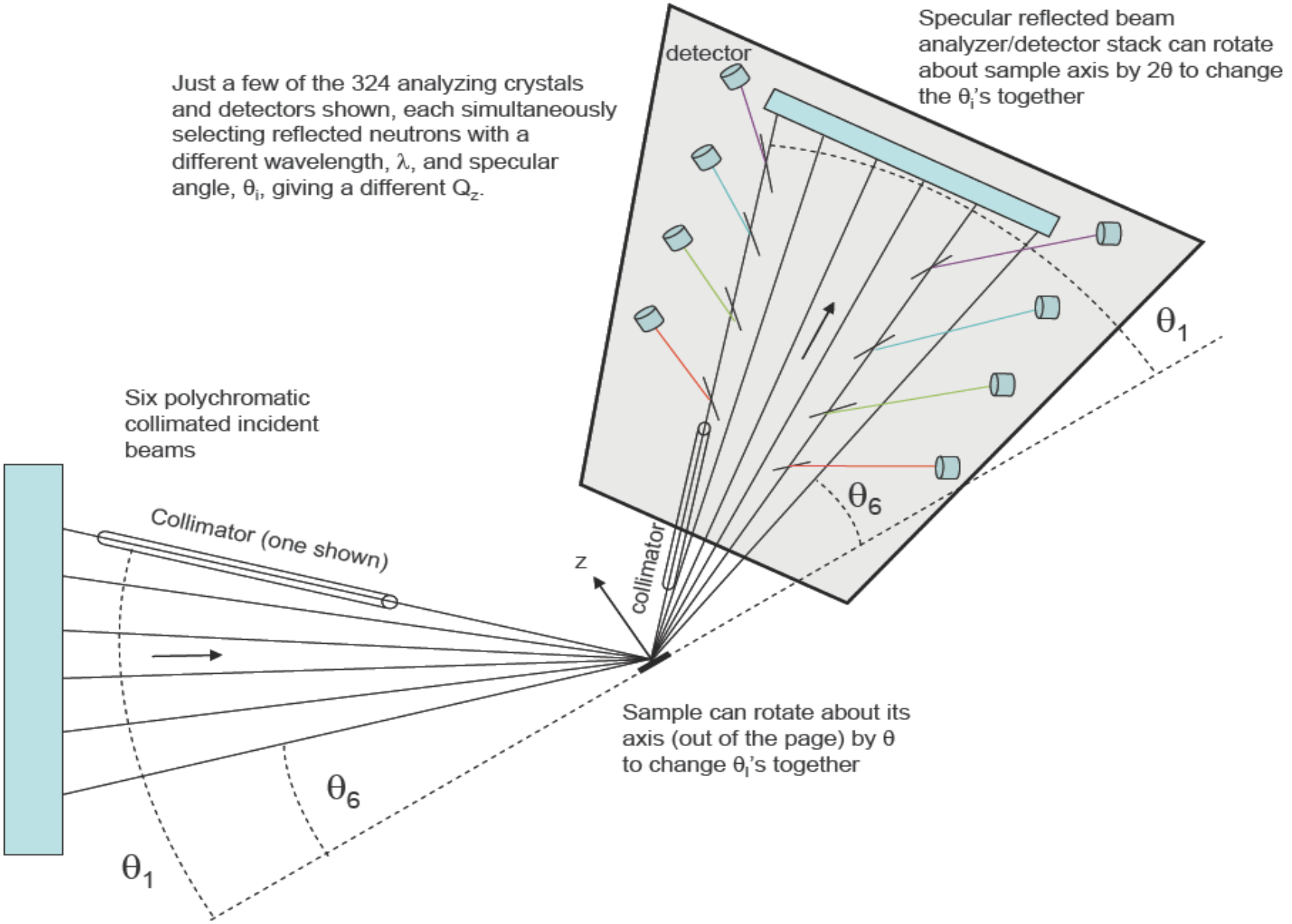

(Thanks to Ron Cappelletti for this slide.)

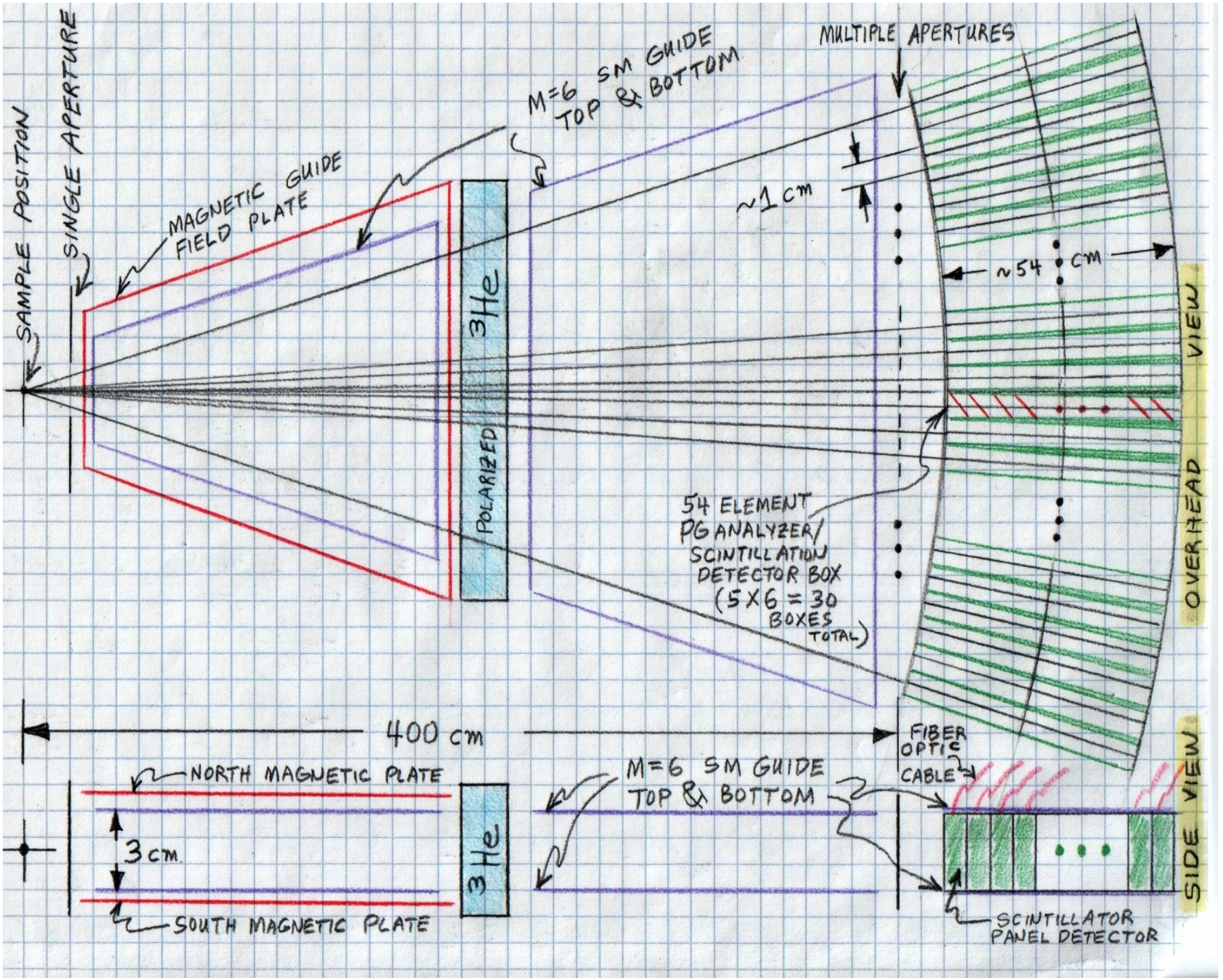
SAMPLE POSITION
SINGLE APERTURE
MAGNETIC GUIDE FIELD PLATE
M=6 SM GUIDE TOP & BOTTOM
MULTIPLE APERTURES
~1 cm
~54 cm
3He
POLARIZED
54 ELEMENT PG ANALYZER/ SCINTILLATION DETECTOR BOX (5X6 = 30 BOXES TOTAL)
OVERHEAD VIEW
400 cm
NORTH MAGNETIC PLATE
3 cm
SOUTH MAGNETIC PLATE
3He
M=6 SM GUIDE TOP & BOTTOM
FIBER OPTIC CABLE
SCINTILLATOR PANEL DETECTOR
SIDE VIEW

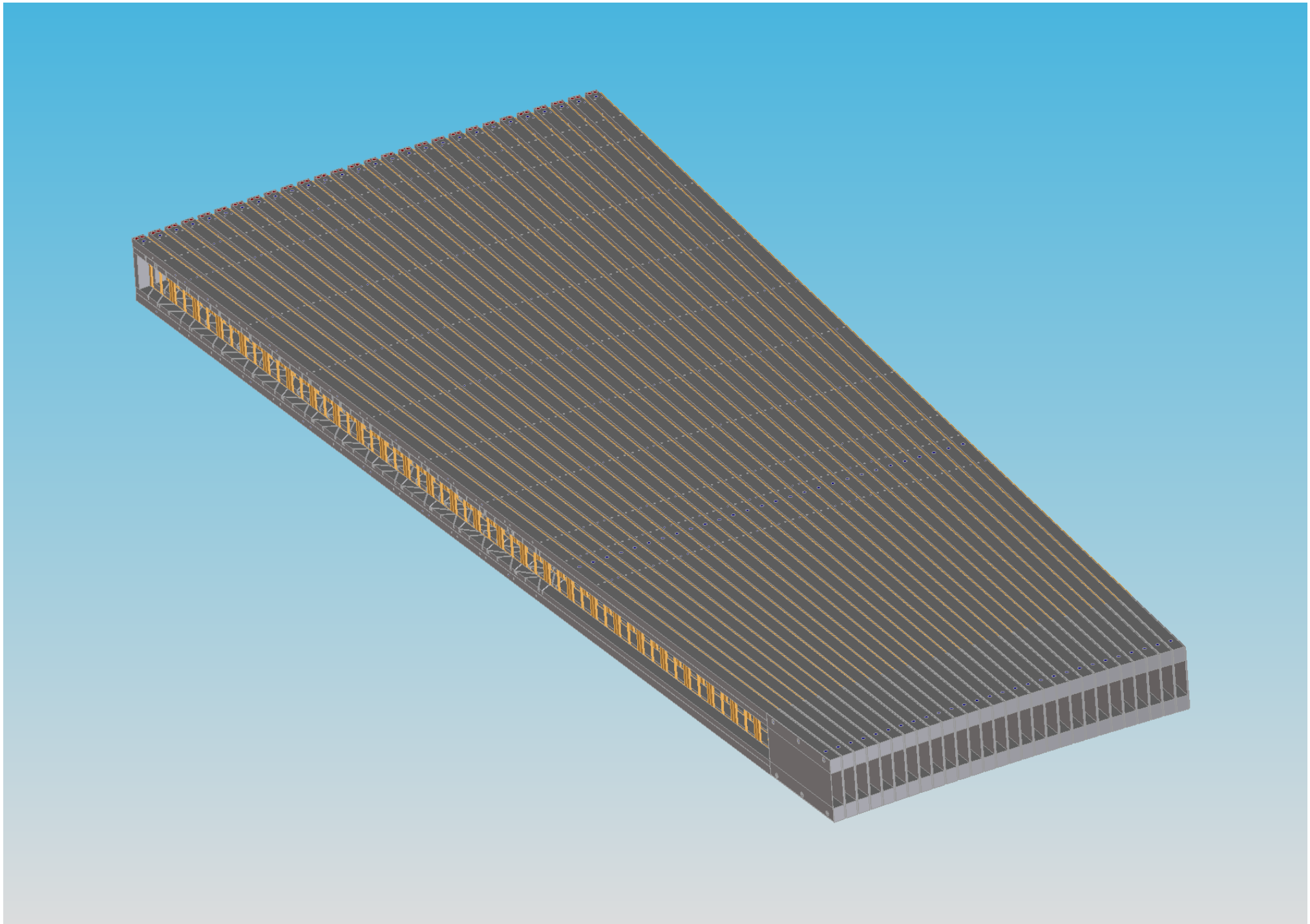

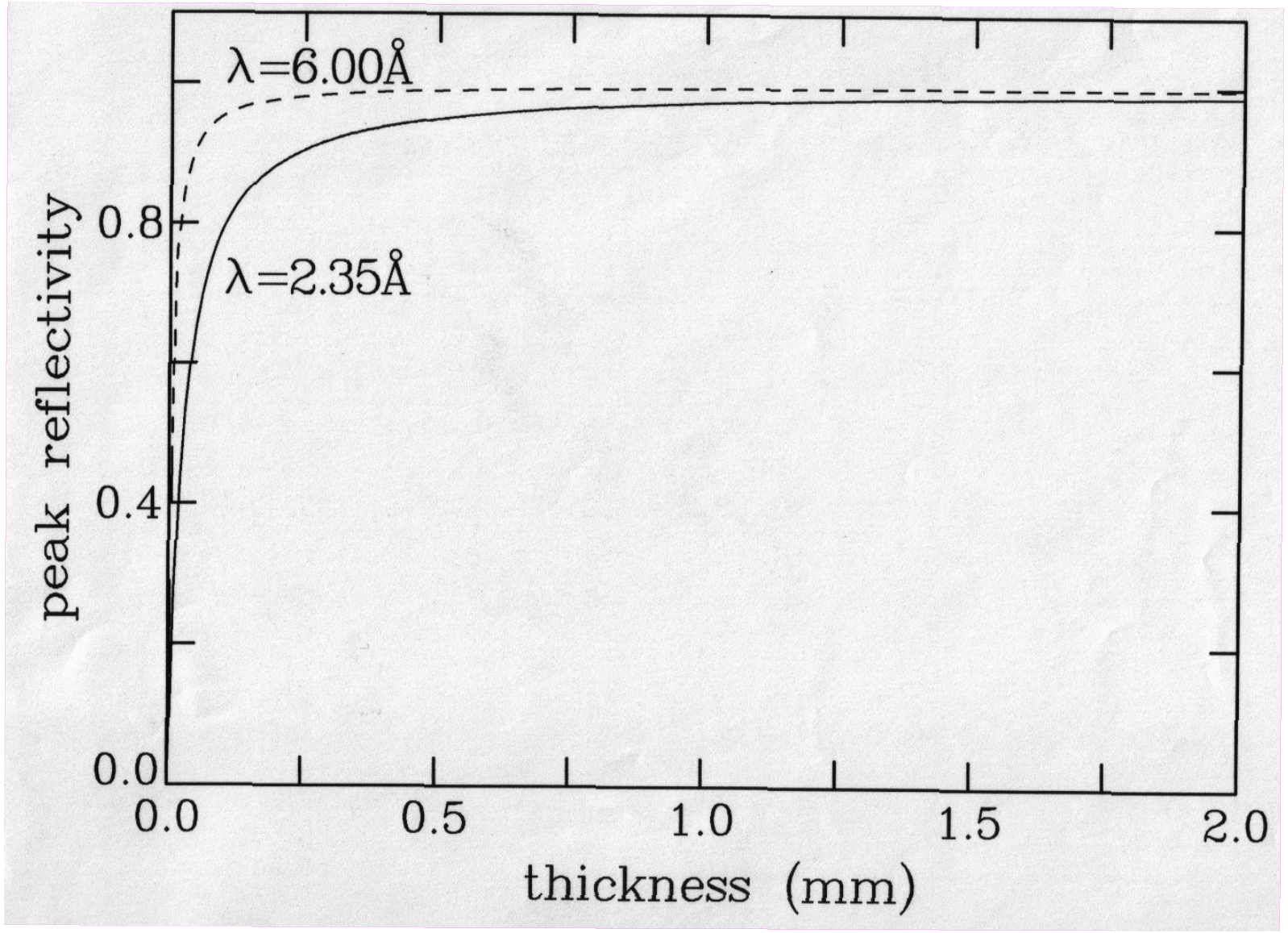

PG (002) crystal with half degree mosaic (from calculations of Dan Neumann).

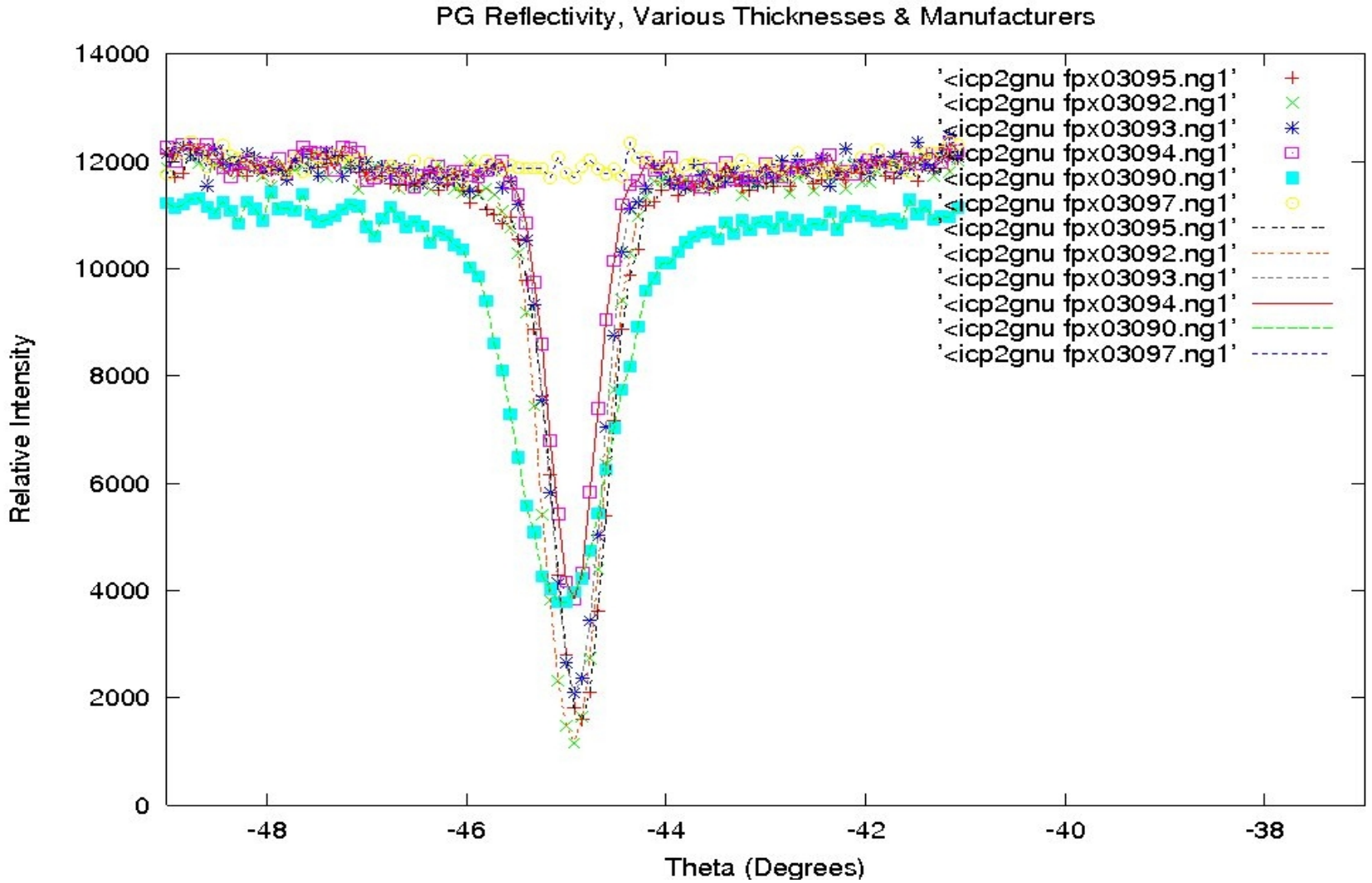

PG(002) samples from Panasonic and other manufacturers. At 5 Angstrom neutron wavelength, the Panasonic samples have mosaic FWHMs of about one half a degree and peak reflectivities of 0.90 and 0.82 for thicknesses of 1 and 0.5 mm, respectively.

Ratio of diffuse to Bragg scattering for pyrolytic graphite crystal
(Measurement performed on the NG-1 polarized beam reflectometer's PG monocromator located on the current NG-1 guide [Be filter in place upstream)].)

The NG-1 focusing monochromator consists of 7 horizontal magnesium “fingers” on each of which are mounted a pair of triple-stacked ZYA grade PG material 50 x 11 x 2 mm thick with mosaic FWHM of about half a degree (the three PG pieces in each stack were slightly inclined relative to one another to give an effective mosaic of approximately 1.31 degrees FWHM).

On the primary Bragg reflection for 4.75 Angstrom neutron wavelength, the measured reflected intensity is approximately 8635. counts/unit time interval compared to a diffuse count of 46. in the same time interval with the monochromator rotated off the Bragg peak by about 1.5 degrees. Neglecting scattering from the magnesium fingers and surrounding air, the ratio of diffuse to Bragg reflected intensity is, conservatively, about 0.0053 or roughly a half a percent. (The beam illuminating the PG monochromator was polychromatic with a Maxwellian distribution determined by the cold source and with a short wavelength cut-off imposed by the upstream Be filter.)

The beam reflected by the sample in which the PG analysers are bathed in the wavelength-dependent detector module for CANDOR is more restricted in comparison (some wavelengths weighted less in general) and the thickness of each PG analyser less (for roughly the same peak reflectivity) -- so the measurement described above represents something of an upper limit.

11 JUN 2007 NG-1 REFLECTOMETER

$\lambda = 4.75$ Å $\Delta\lambda/\lambda \simeq 0.01$ SLITS: 0.5/0.25/2.0/0.5 mm

TRANSMISSION THROUGH PG FILTER MATERIAL

(≥ 1⅝ INCHS THICK)(BEAM ⊥ (002) PLANES)

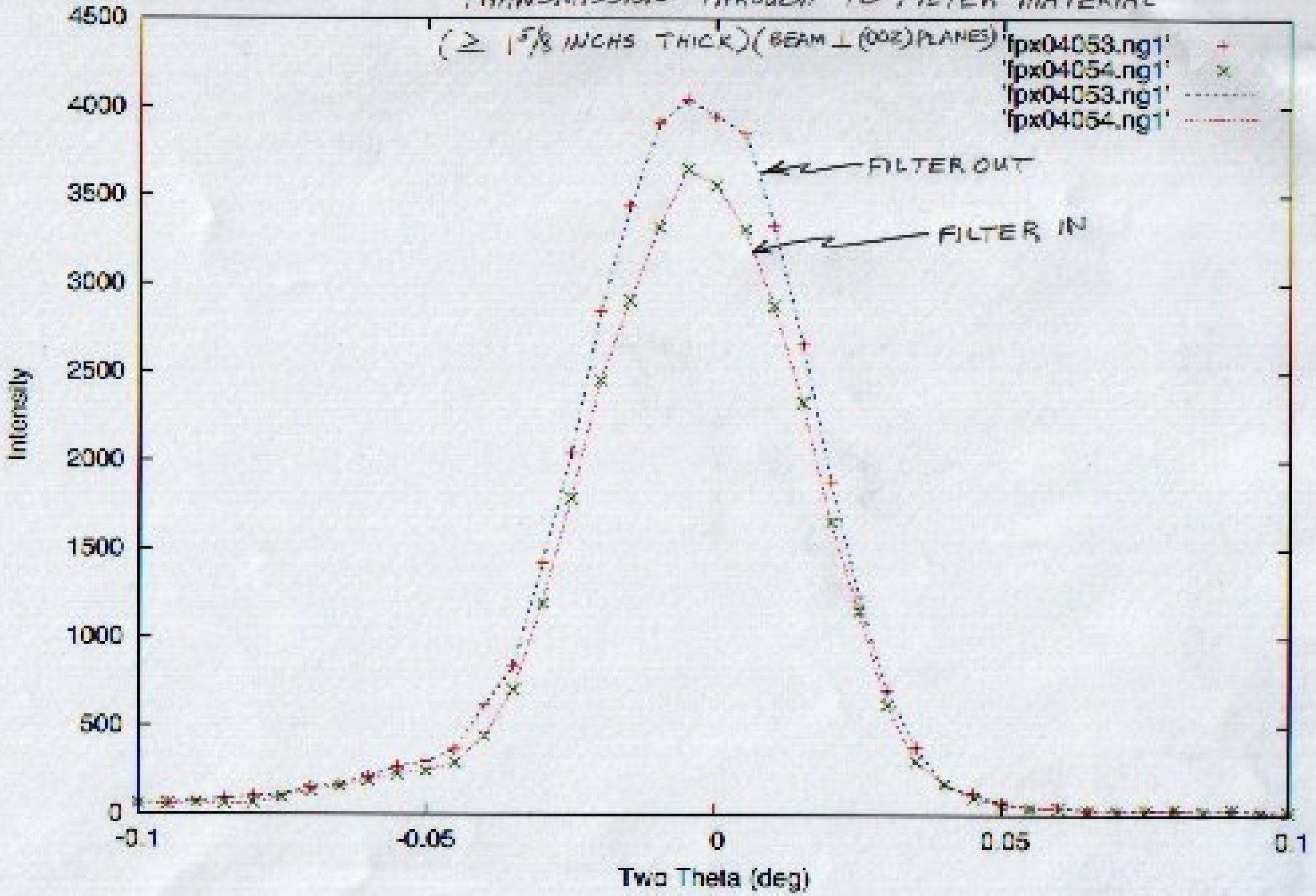

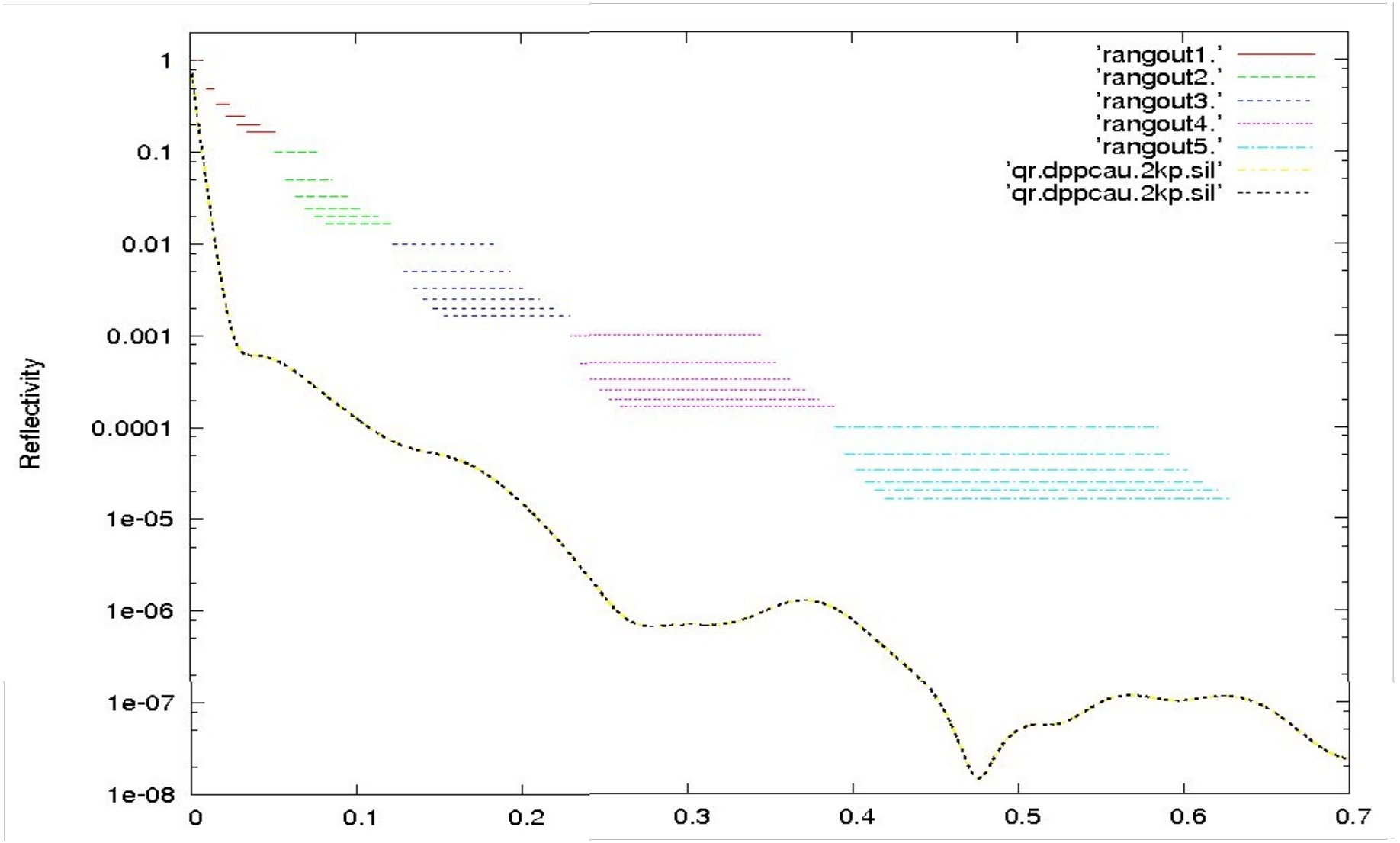

Sample neutron reflectivity curve with the ranges that each of the six distinct beams will cover in Q (horizontal scale in inverse Angstroms) for a wavelength band from 4 to 6 Angstroms. The vertical placement of the Q ranges is for clarity only. Each group of ranges corresponds to a different orientation of the sample relative to the incident beams.

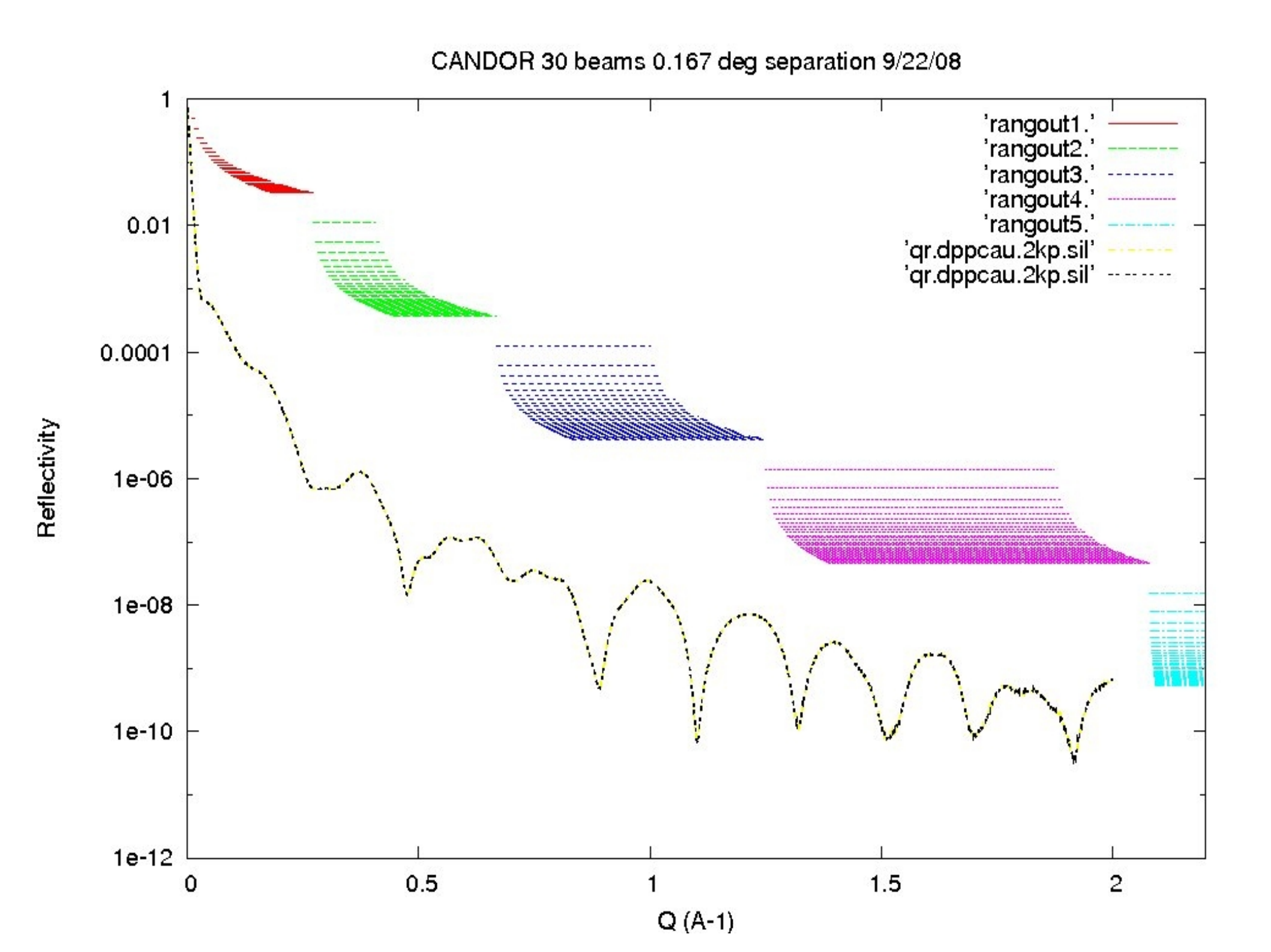
CANDOR 30 beams 0.167 deg separation 9/22/08
Reflectivity
Q (A-1)
1
0.01
0.0001
1e-06
1e-08
1e-10
1e-12
0
0.5
1
1.5
2
'rangout1.'
'rangout2.'
'rangout3.'
'rangout4.'
'rangout5.'
'qr.dppcau.2kp.sil'
'qr.dppcau.2kp.sil'

NCNR FACILITY

ca. 2015

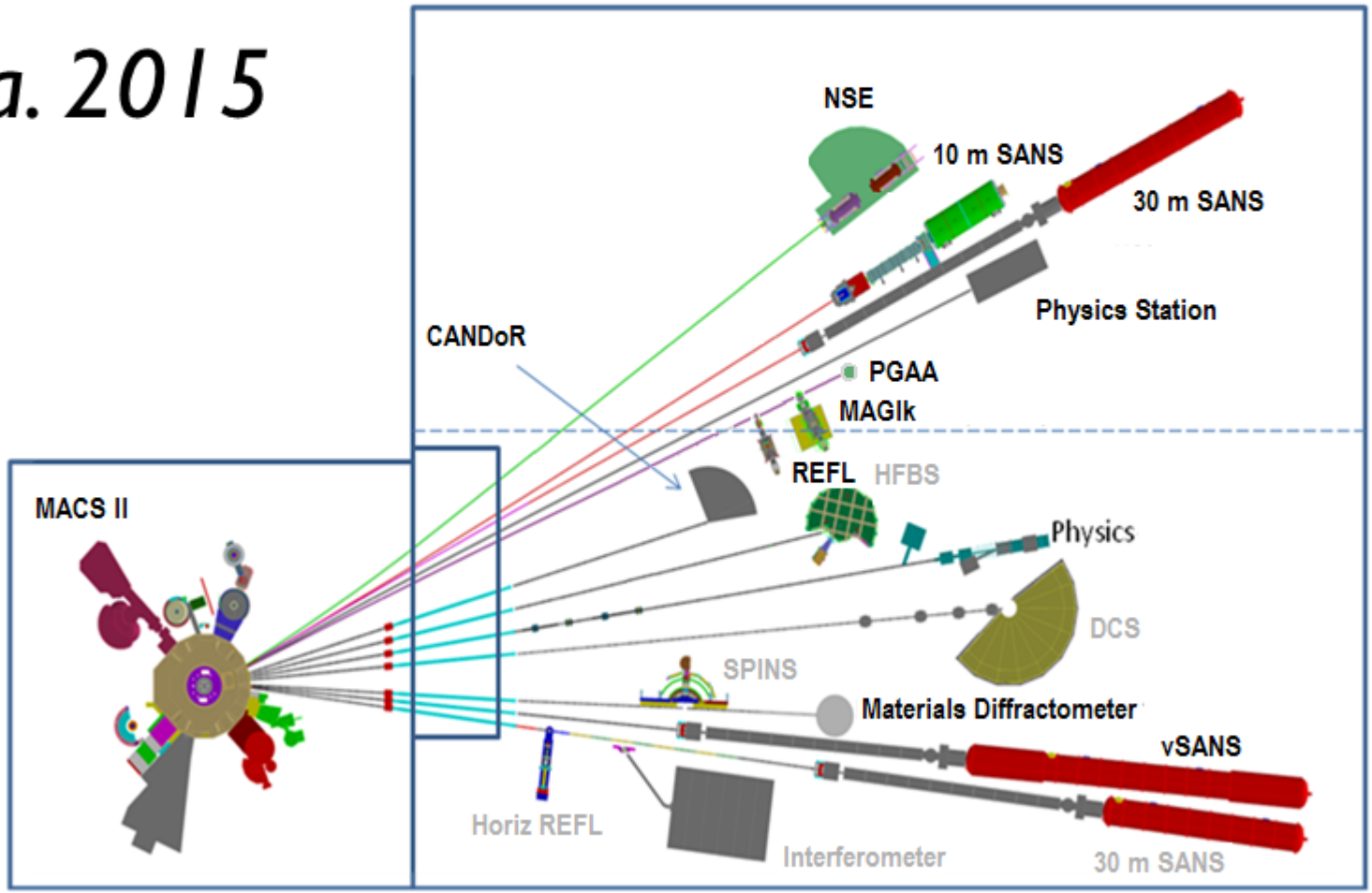

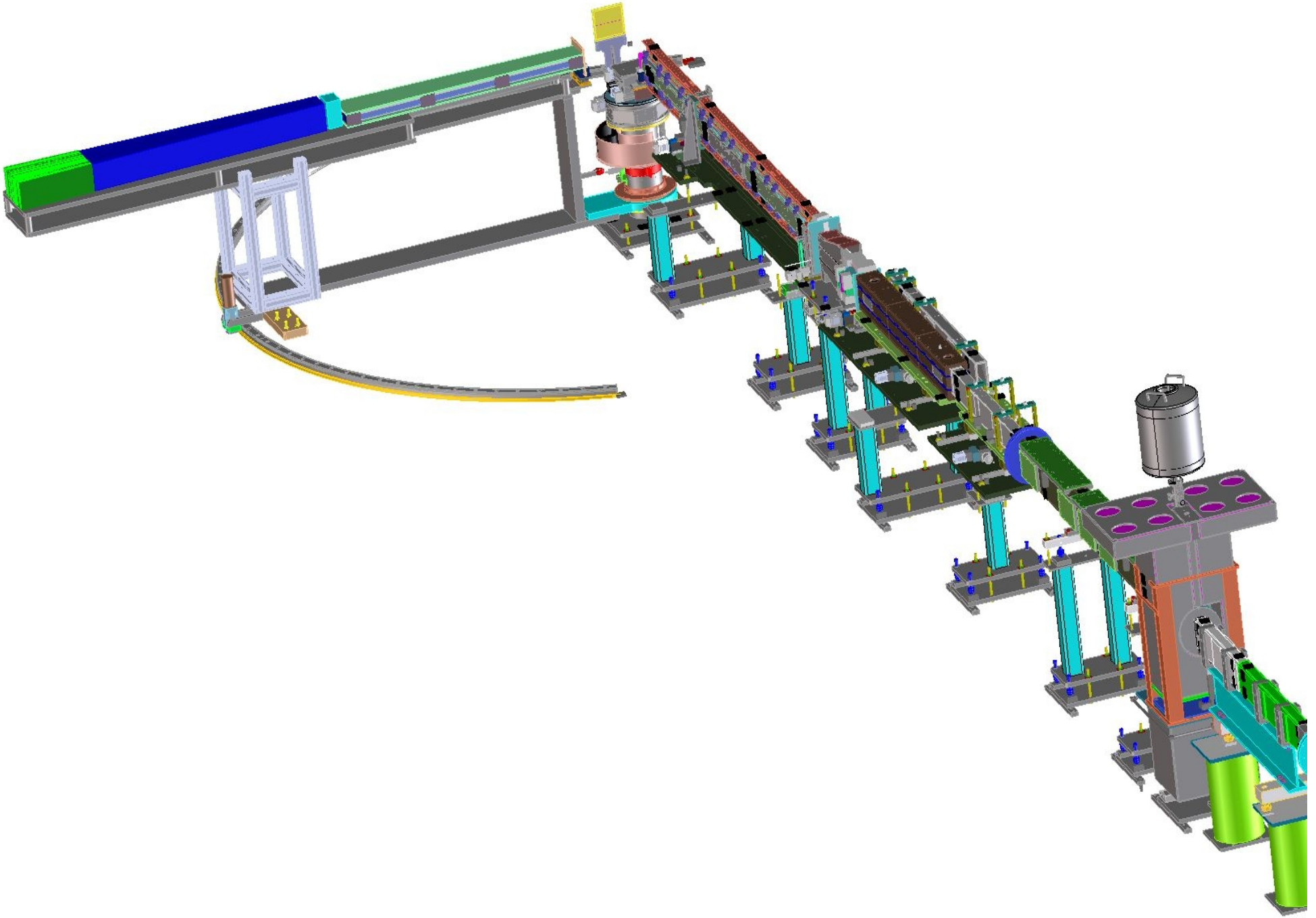

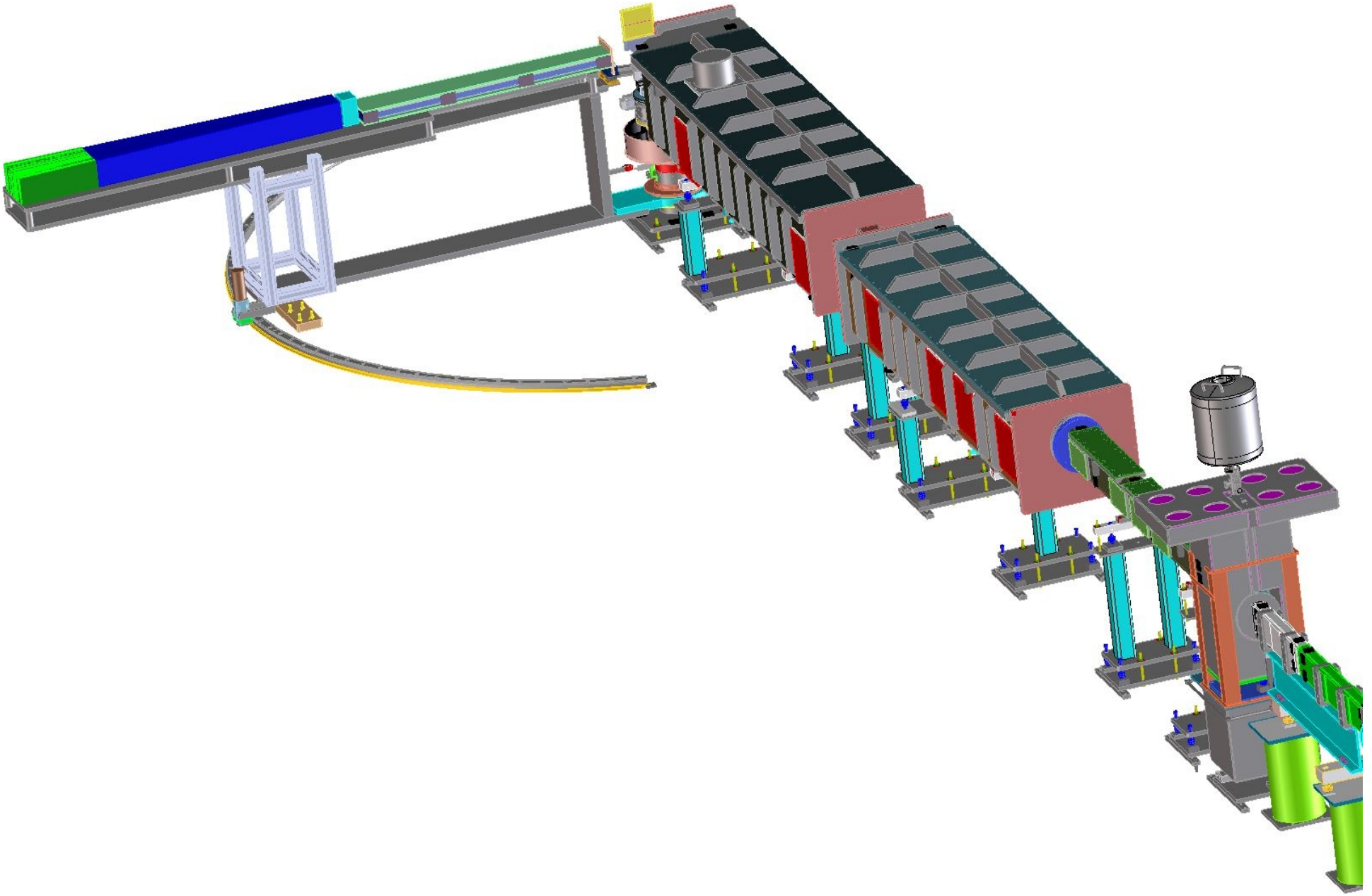

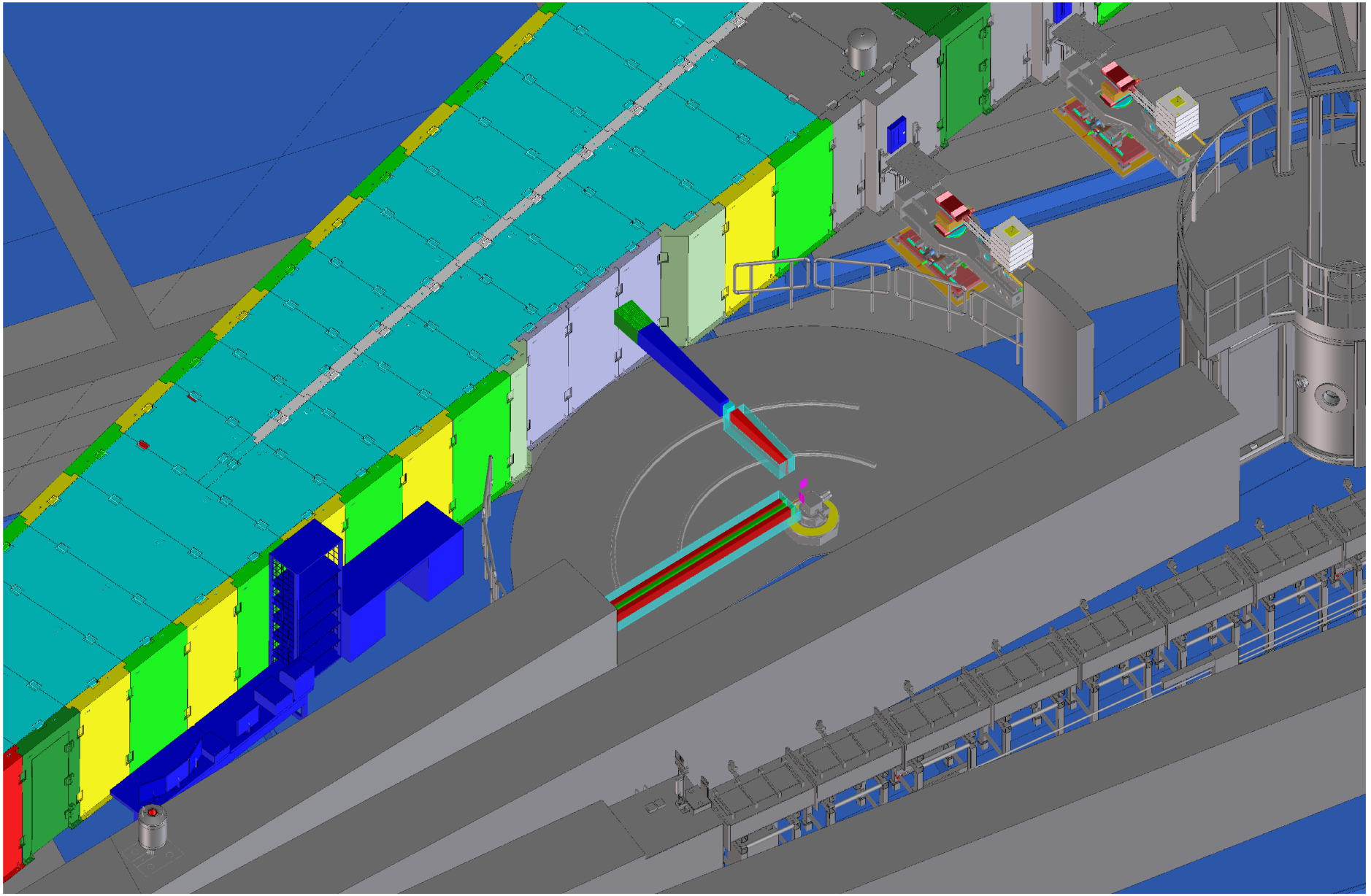

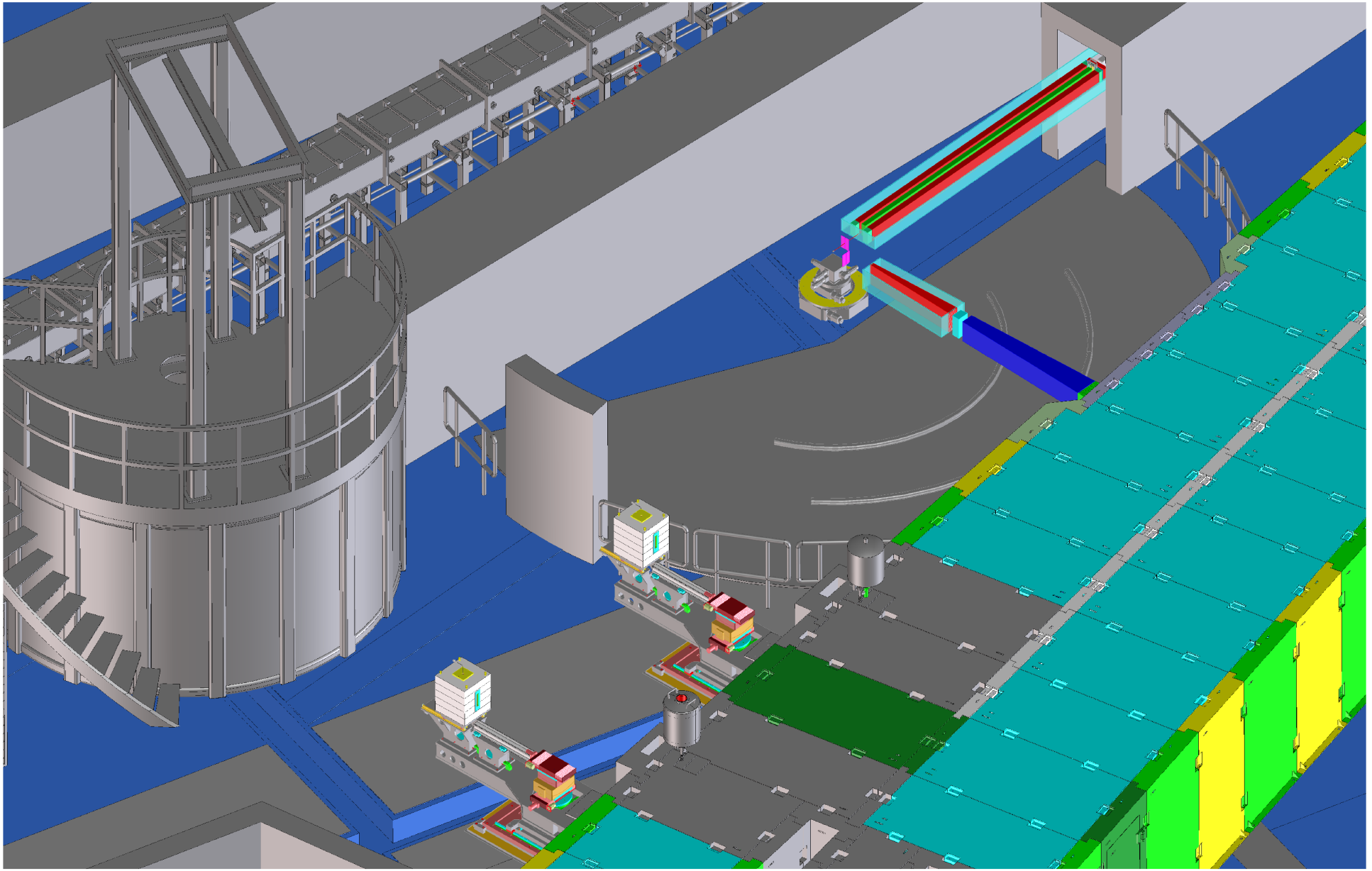

Polychromatic energy-dispersive neutron diffraction at a continuous source

Jason M. Simmons, Jeremy C. Cook, Richard M. Ibberson, Charles F. Majkrzak and Dan A. Neumann

J. Appl. Cryst. (2013). **46**, 1347–1352

We present a design for a continuous source, polychromatic beam powder neutron diffractometer based on an energy-dispersive detection methodology. Such an instrument would offer significantly higher incident neutron flux, with an attendant increase in data collection rate, reducing the time per scan from hours to seconds. Completely passive components are conceived for neutron bandwidth shaping and detection is achieved using a massively parallel analyser/detector system, making installation and operation of the instrument comparatively simple. The proposed instrument is intended to be used for rapid structural characterisations of small samples or for kinetic studies of materials undergoing structural or magnetic phase changes.

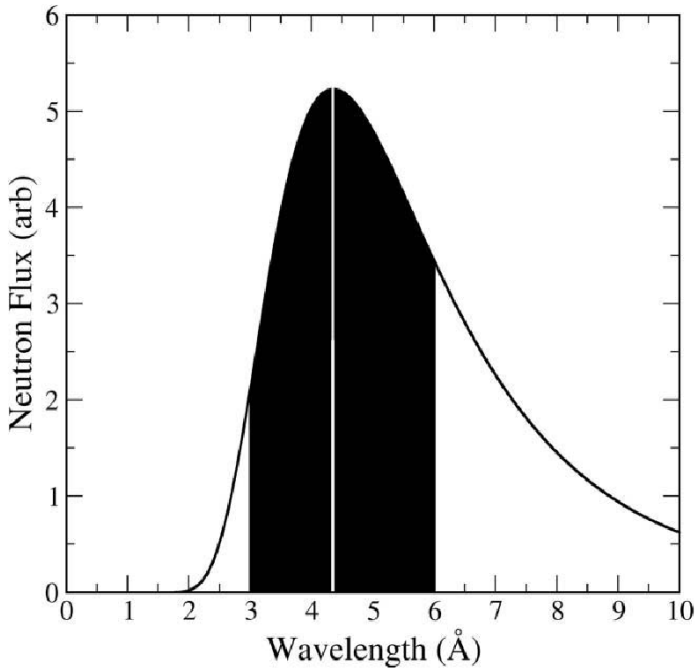

Figure 1
Schematic cold neutron flux using a Maxwell–Boltzmann distribution at 20 K. The black area represents the incident neutron flux for the proposed instrument as compared with the incident flux for a monochromatic neutron powder diffractometer with $\Delta\lambda/\lambda \simeq 0.2\%$, shown as a white line at the peak in the neutron spectrum.

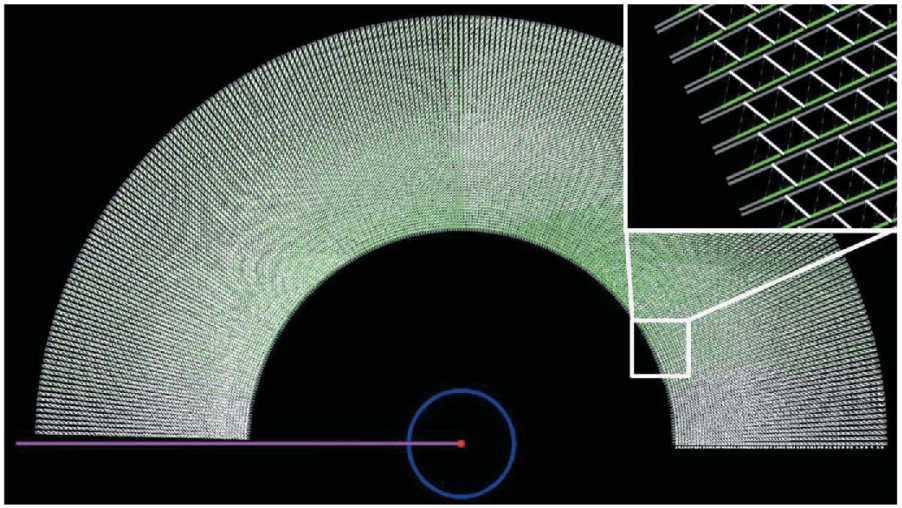

Figure 2
Diagram of the proposed MD instrument consisting of ~230 banks of analyzer/detector modules covering a scattering angle between ~0 and 179°. Such an assembly would contain more than 10 000 independent detectors. The incident neutrons are shown as a pink beam which diffracts from the red cylindrical sample at the center. The blue circle represents the sample environment (*e.g.* cryostat) that encloses the sample. Inset: close-up view of the entrance to an array of analyzer/detector banks, showing the dense packing of independent PG analyzer crystals in white and neutron detectors in green. A more detailed schematic of the PG analyzer crystals and corresponding scintillation detector plates is shown in Fig. 4.

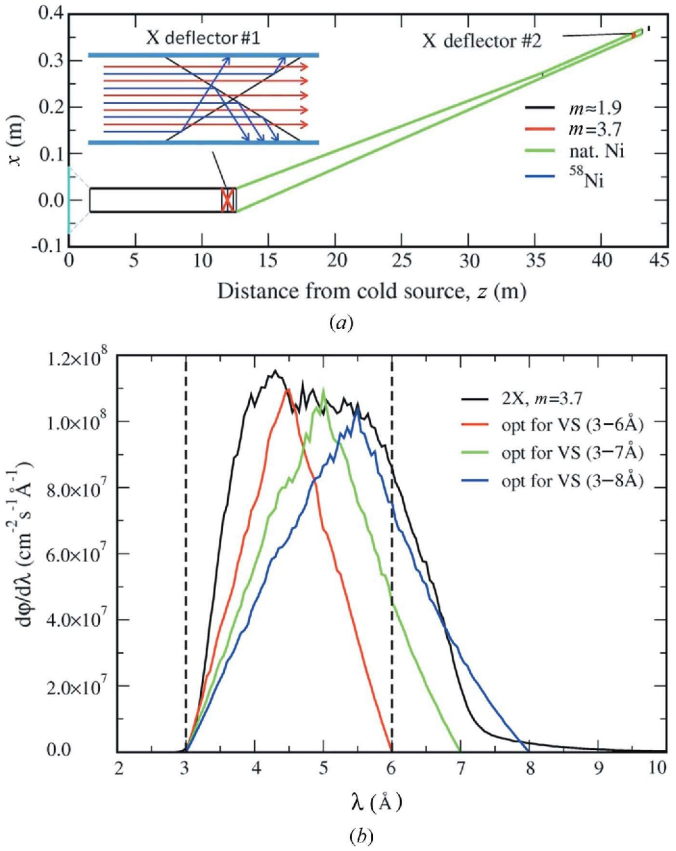

Figure 3
(*a*) Plan view of the proposed wavelength band shaping filters, with two X deflector/supermirrors installed within the guide. The X deflectors remove low-energy neutrons (blue) from the beam, shown schematically in the upper inset, while the green guide component acts as a low-energy bandpass optical filter. (*b*) Comparison of methods to shape the incident cold neutron beam, with the proposed passive elements in black, and different velocity selector (VS) settings in red, green, and blue. Each curve represents the flux for a given system allowing for full optimization of the guide properties as well as of the velocity selector or optical filter/X supermirror design. The passive optical filter and X supermirrors offer rigorous neutron rejection for $\lambda < 3$ Å, while also providing the most rectangular spectrum covering the desired $3 < \lambda \leq 6$ Å bandwidth.

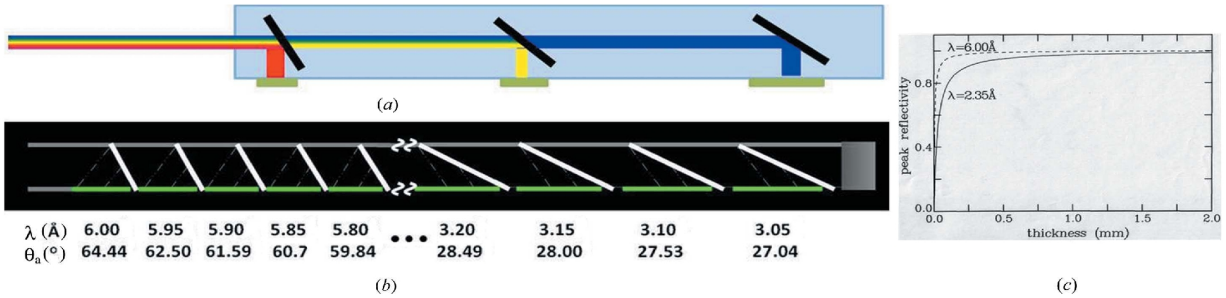

Figure 4
(*a*) Schematic concept for energy dispersive neutron detection where the diffracted polychromatic beam passes through a series of analyzer crystals. The analyzers are set to select a single wavelength from the beam with high reflectivity but low absorption of the shorter-wavelength neutrons which will continue down the channel. (*b*) Detail of a single analyzer/detector channel, showing the arrangement of each PG analyzer crystal (white) and scintillation detector (green). (*c*) Calculated PG reflectivity as a function of analyzer thickness, showing >90% reflectivity for neutrons in the MD bandwidth.

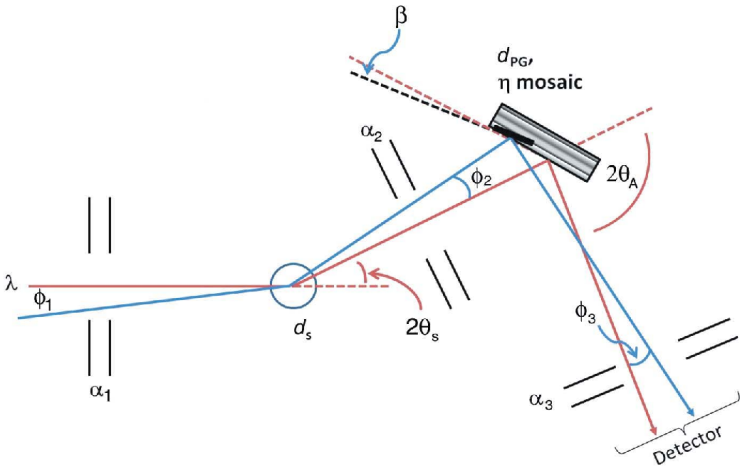

Figure 5
Geometry of an energy-dispersive neutron diffractometer, where λ is a single wavelength within the incident, polychromatic, neutron spectrum that diffracts from the powder sample with d spacing d_s, is energy analyzed (diffracted) by a PG crystal with d spacing d_{PG} and mosaicity η, and is directed towards the neutron detector. The presample, sample–analyzer and analyzer–detector collimations are α_1, α_2 and α_3, respectively, and represented by a pair of slits. The red lines show the path of a perfectly aligned neutron which diffracts to an angle $2\theta_s$ and is energy analyzed by diffracting to an angle $2\theta_A$. The blue paths show a misaligned neutron, with angular dispersion through each collimator represented by the angle ϕ_i, which is diffracted by a crystallite within the PG analyzer that is misaligned by an angle β with respect to the nominal c axis.

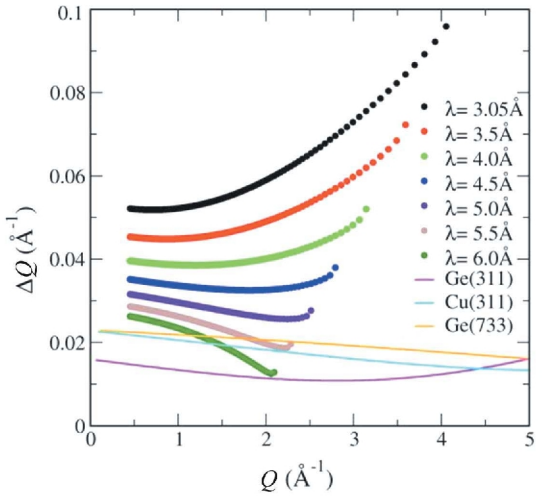

(*a*)

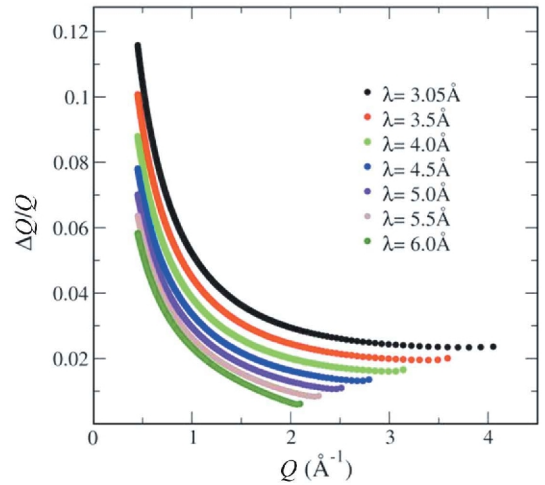

(*b*)

Figure 6
Calculated momentum-transfer (Q) resolution for the MD, plotted in (*a*) absolute and (*b*) relative units and as a function of the wavelength of the neutron. By comparison, the absolute Q resolution available for each monochromator on the BT1 diffractometer at the NCNR, with 15′ incident collimation, is plotted over the analogous Q range. The MD offers comparable resolution to BT1 for the 4–6 Å bandwidth where the incident flux is highest. In relative terms, $\Delta Q/Q$ is less than 10% for the full Q range and less than 5% for $1 < Q < 4$ Å^{-1}.

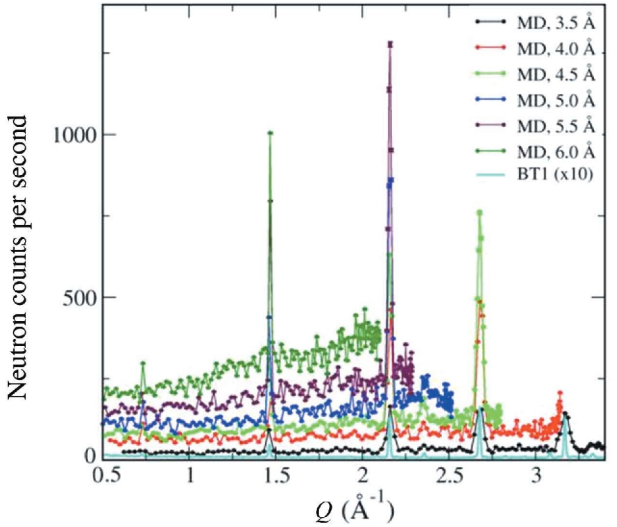

(*a*)

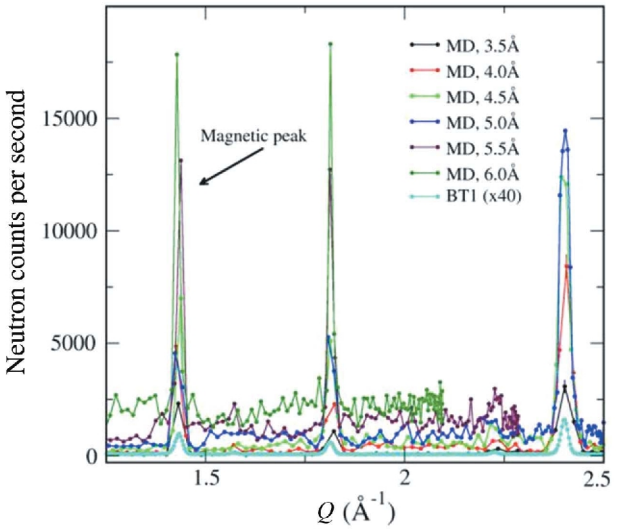

(*b*)

Figure 7
Monte Carlo simulated neutron count rate for the MD compared with experimental data collected on BT1. (*a*) NdOFeAs pnictide superconductor, with experimental data collected over 7 h using neutrons with a wavelength of 2.087 Å. (*b*) Low-Q portion of the diffraction pattern for $SrFeO_2$ in the antiferromagnetic state, with the lowest Q magnetic diffraction peak indicated. These data were collected over 6 h using neutrons with a wavelength of 1.54 Å. To be visible on the same scale as the MD, the experimental BT1 diffraction patterns were multiplied by 10 and 40, respectively.

Scintillation Detector Technical Details Presented in Posters at the ACNS in Knoxville, June 2014

BP3.11

Neutron Detector Optimization using GEANT 4 Simulation Software Yaacov Yehuda-Zada[1,2] Itzhak Orion[2], Nicholas C, Maliszewskyj[3], Alon Osovizky[3,4]; [1]BGU, Beer Sheva, Israel; [2]NRCN, Beer-Sheva , Israel; [3]NIST, Gaithersburg, Maryland; [3]Rotem Industries Ltd, Rotem Industrial Park, Israel.

BP2.07

A Real-Time Neutron/Gamma Discrimination Algorithm for a Low Cost LiF:ZnS(Ag) Neutron Detector Kevin Pritchard[1], Alon Osovizky[1,2], Nicholas Maliszewskyj[1], Jeffrey Ziegler[1] and Charles Majkrzak[1]; [1]NIST Center for Neutron Research, Gaithersburg, Maryland; [2]Rotem Industries Ltd, Rotem Industrial Park, Israel.

BP3.11

Design Constraints and Optimization of a 6LiF:ZnS(Ag) based Neutron Detector Alon Osovizky[1,2] Kevin Pritchard[1], Jeffrey B. Ziegler[1], Yaacov Yehuda-Zada[3,4] Nicholas C. Maliszewskyj[1], Charles F. Majkrzak[1]; [1]NIST, Gaithersburg, Maryland; [2]Rotem Industries, Rotem Industrial Park, Israel; [3]NRCN, Beer Sheva, Israel; [4]BGU, Beer Sheva, Israel.

Detection Mechanism

6LiF:ZnS(Ag)

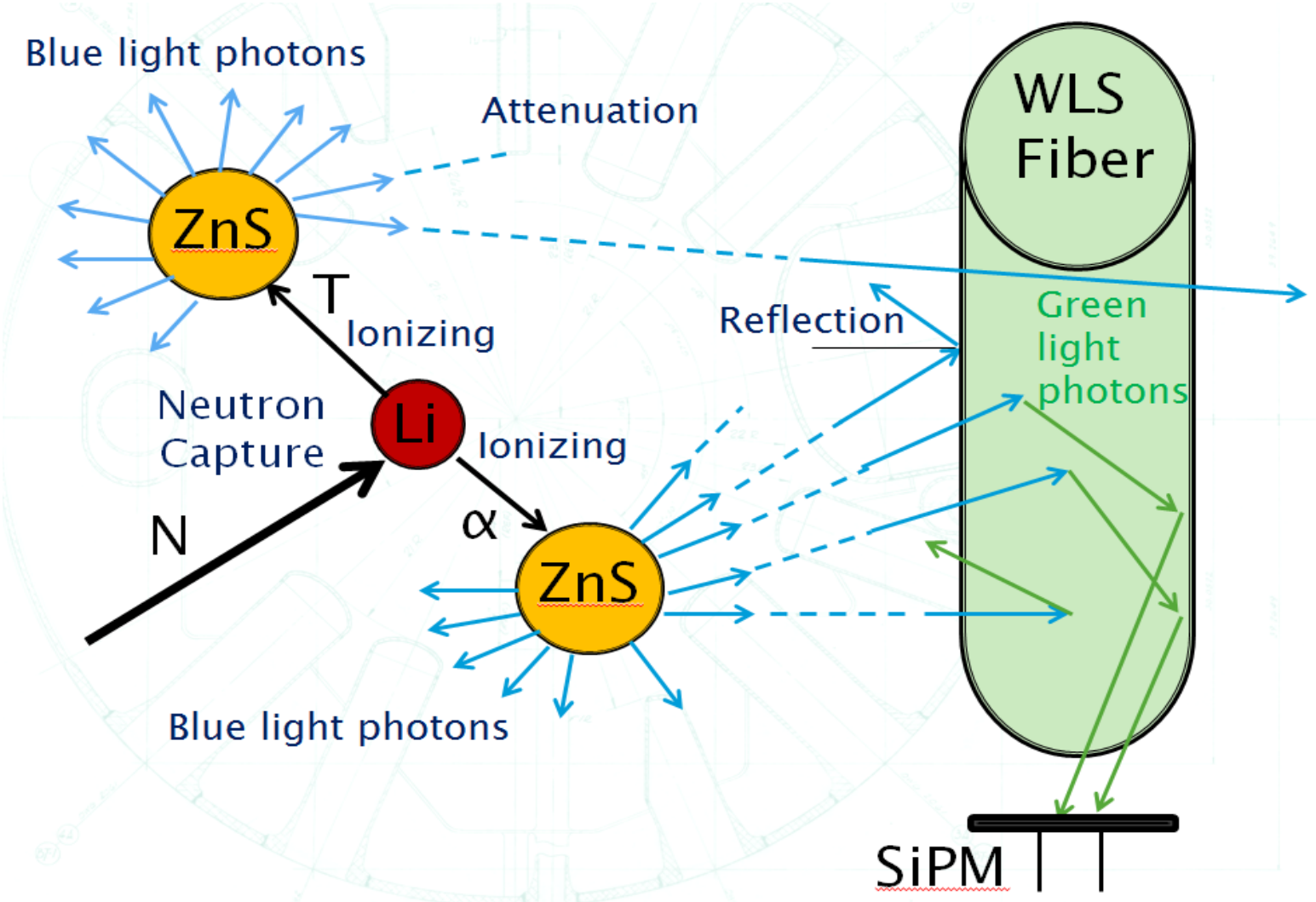

SiPM photodetector

<> A silicon photomultiplier is a 2D array of avalanche photodiodes or “pixels”.
<> One pixel discharges per photon event with a gain of ~10^6
<> This creates an interpretable signal from just a handful of photons
<> However, thermal excitation can form electron-hole pairs too … just like photons.
<> Thermal noise is a major problem that makes identifying neutron more events difficult

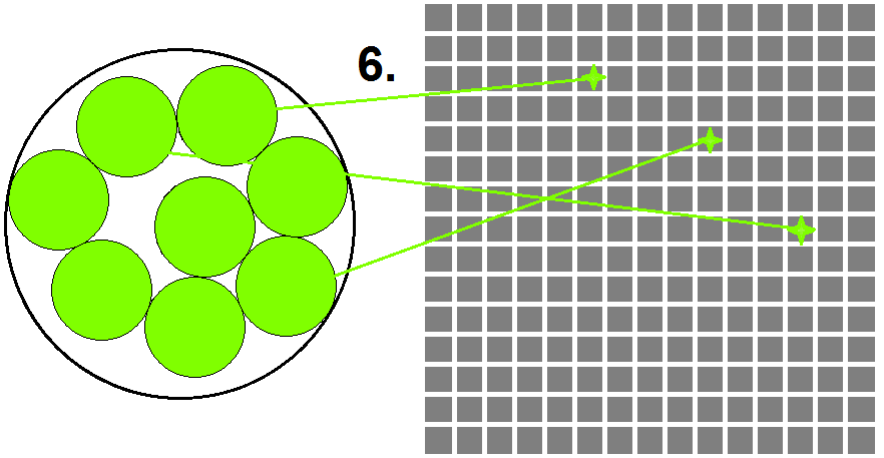

Optimization of Detector Composition and Geometry

Stopping Power vs. Light Output -- 6LiF to ZnS(Ag) ratio

<> more Lithium will capture more neutrons

but

<> more Zinc-Sulfide will yield more light

Light Transport

<> add reflectors to the scintillator surface

<> optimal dye concentration in WLS fibers

<> effects of grain size and homogeneity

<> ratio of WLS fiber volume to that of 6LiF and ZnS(Ag)

A working prototype consists of :

- LiFZnS(Ag) scintillator (Eljen)
- WLS fibers (Kuraray)
- SiPM light Sensor (SensL)
- Self design front-end electronic
- ADC+FPGA based measuring system

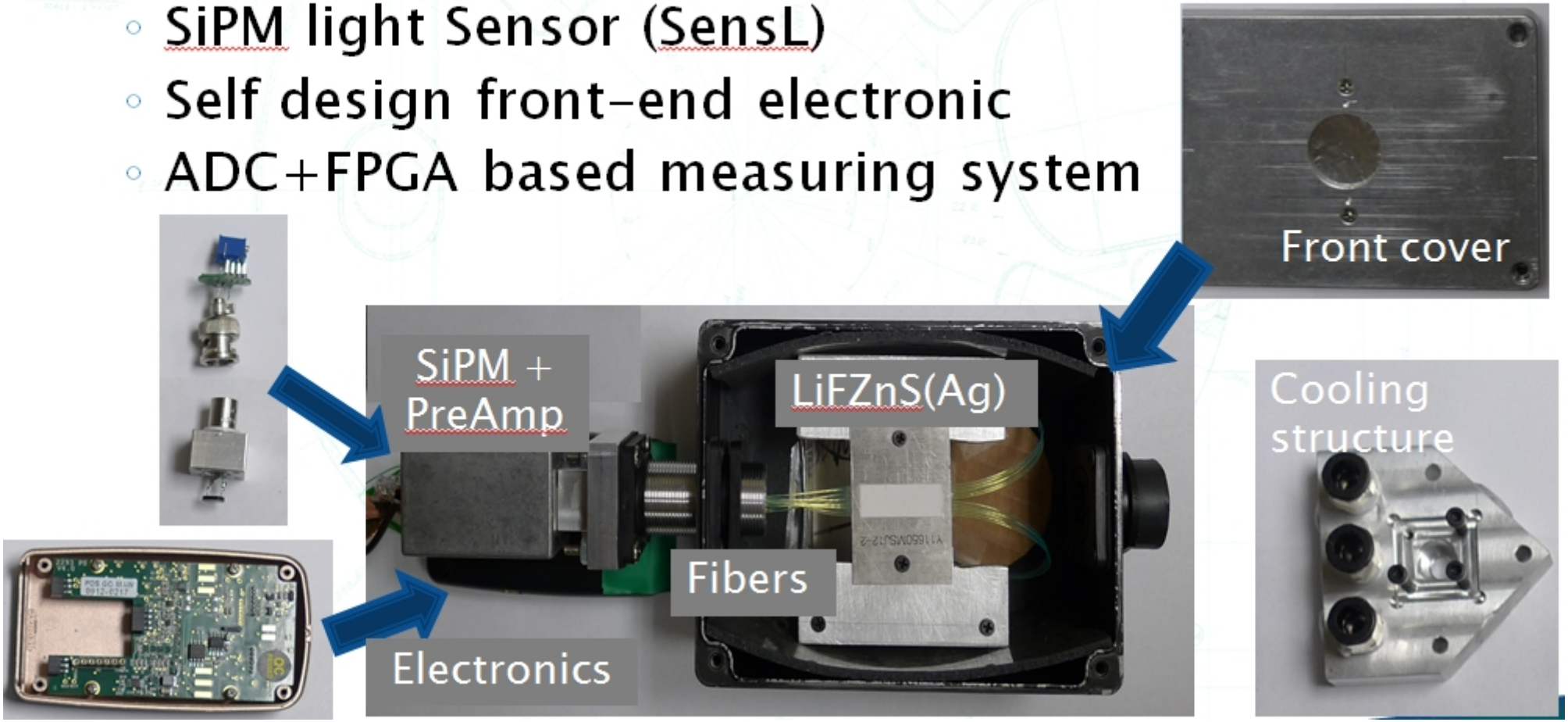

LiF:ZnS:Binder Compound

Sensitivity

- Weight ratio
  - Neutron capture (Li)
  - Light output (ZnS)
  - Light attenuation (Transparency) (ZnS) and (Binder)
  - homogenous mixture (Binder)
- Fibers Volume
- Reflector
- Grain Size
- Light Sensor properties

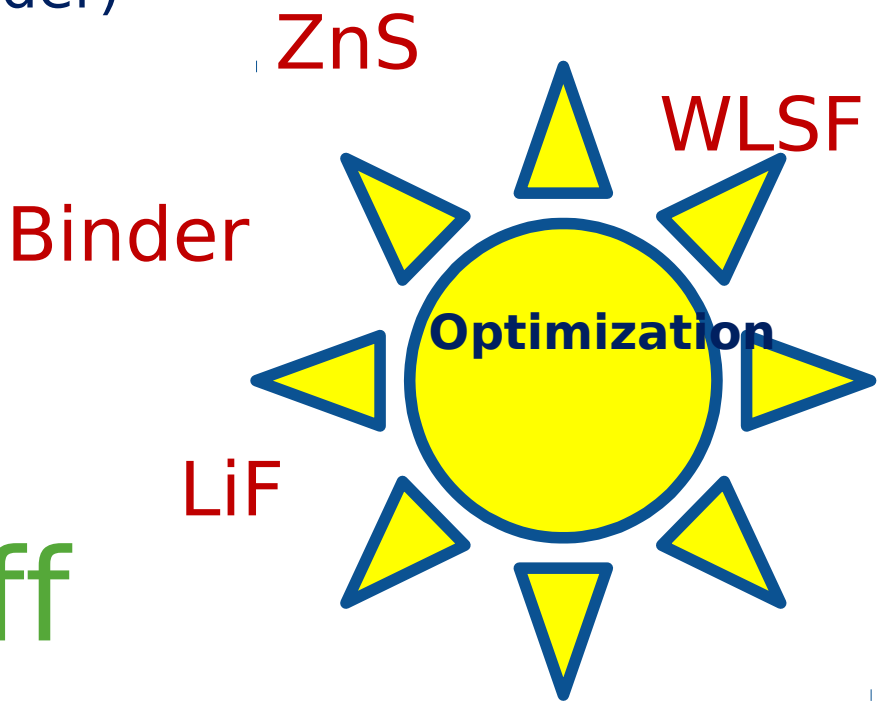

Trade-off

Simulation - Light collection by WLS fiber

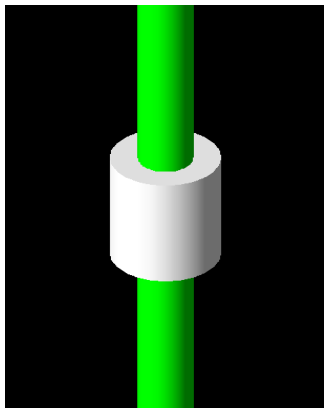

Side View

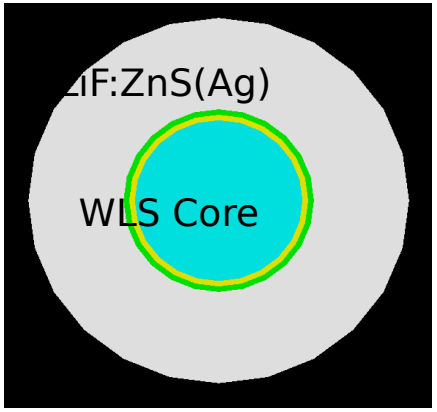

1:3:0.3

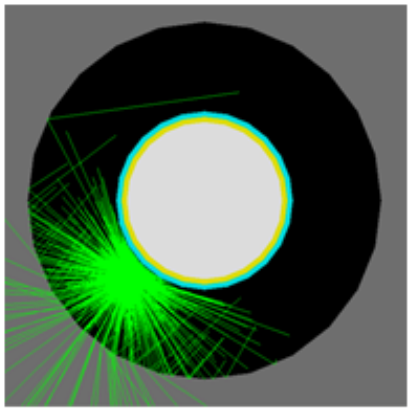

Distance = 0.3 mm
Light reaching WLS = 15.79%

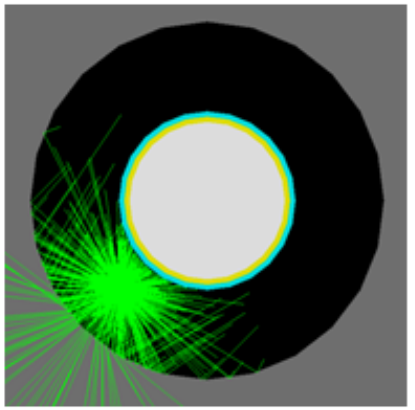

Distance = 0.35 mm
Light reaching WLS = 7.64%

51.61% light loss when double the distance

1:2:0.3

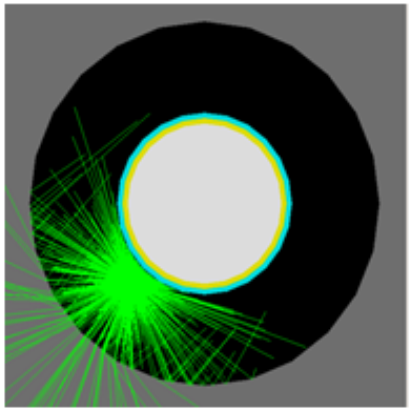

Distance = 0.3 mm
Light reaching WLS = 16.88%

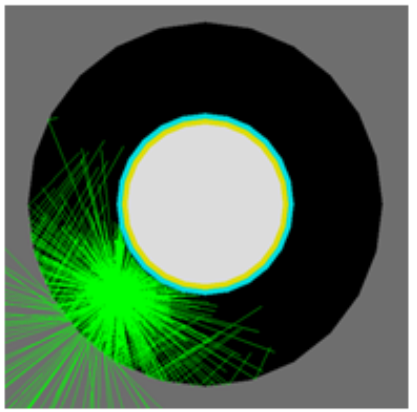

Distance = 0.35 mm
Light reaching WLS = 8.63%

48.87% light loss when double the distance

Grain Size

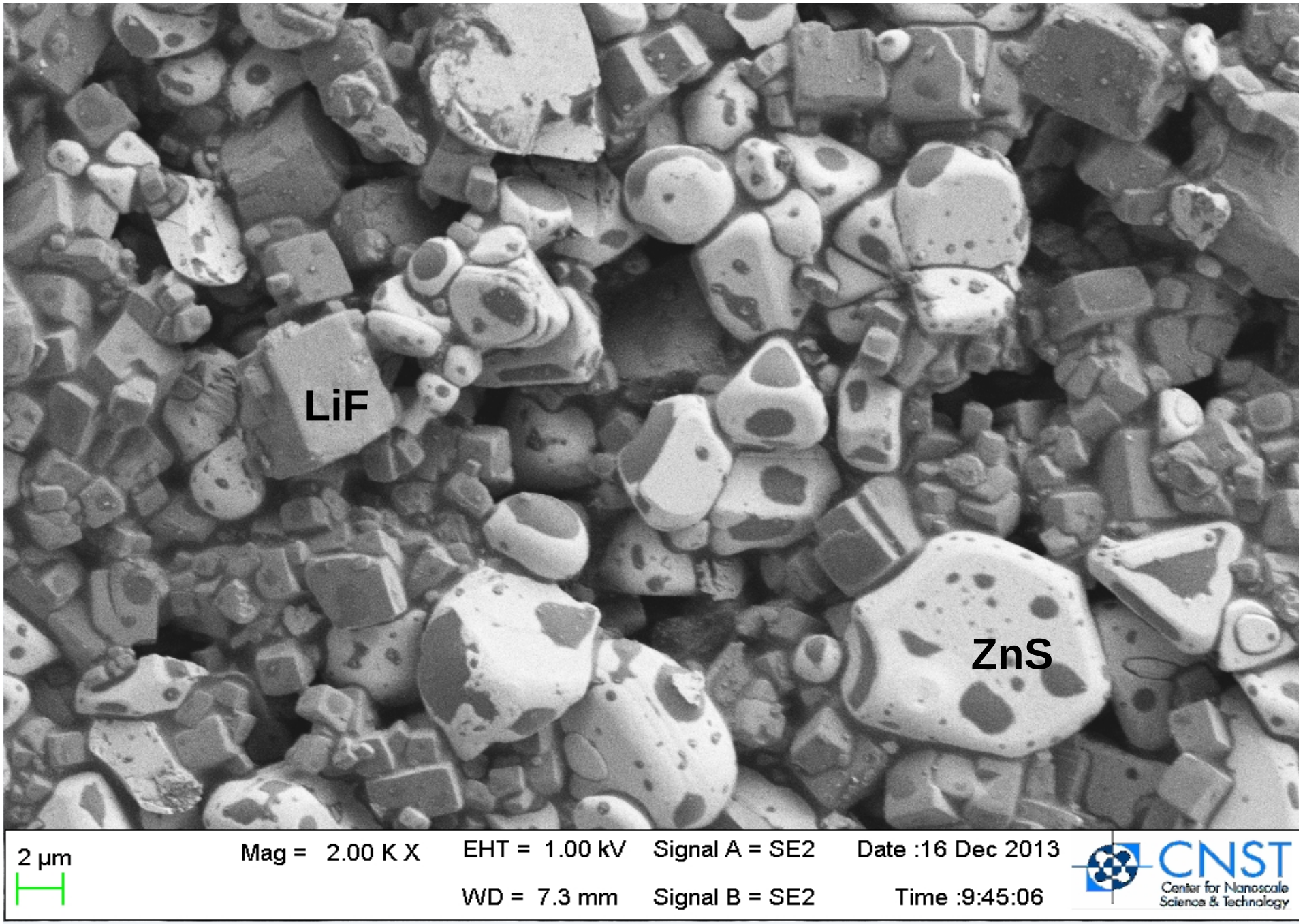
LiF
ZnS
2 µm
Mag = 2.00 K X
EHT = 1.00 kV
WD = 7.3 mm
Signal A = SE2
Signal B = SE2
Date :16 Dec 2013
Time :9:45:06
CNST
Center for Nanoscale Science & Technology

Compound Optimization - Grains

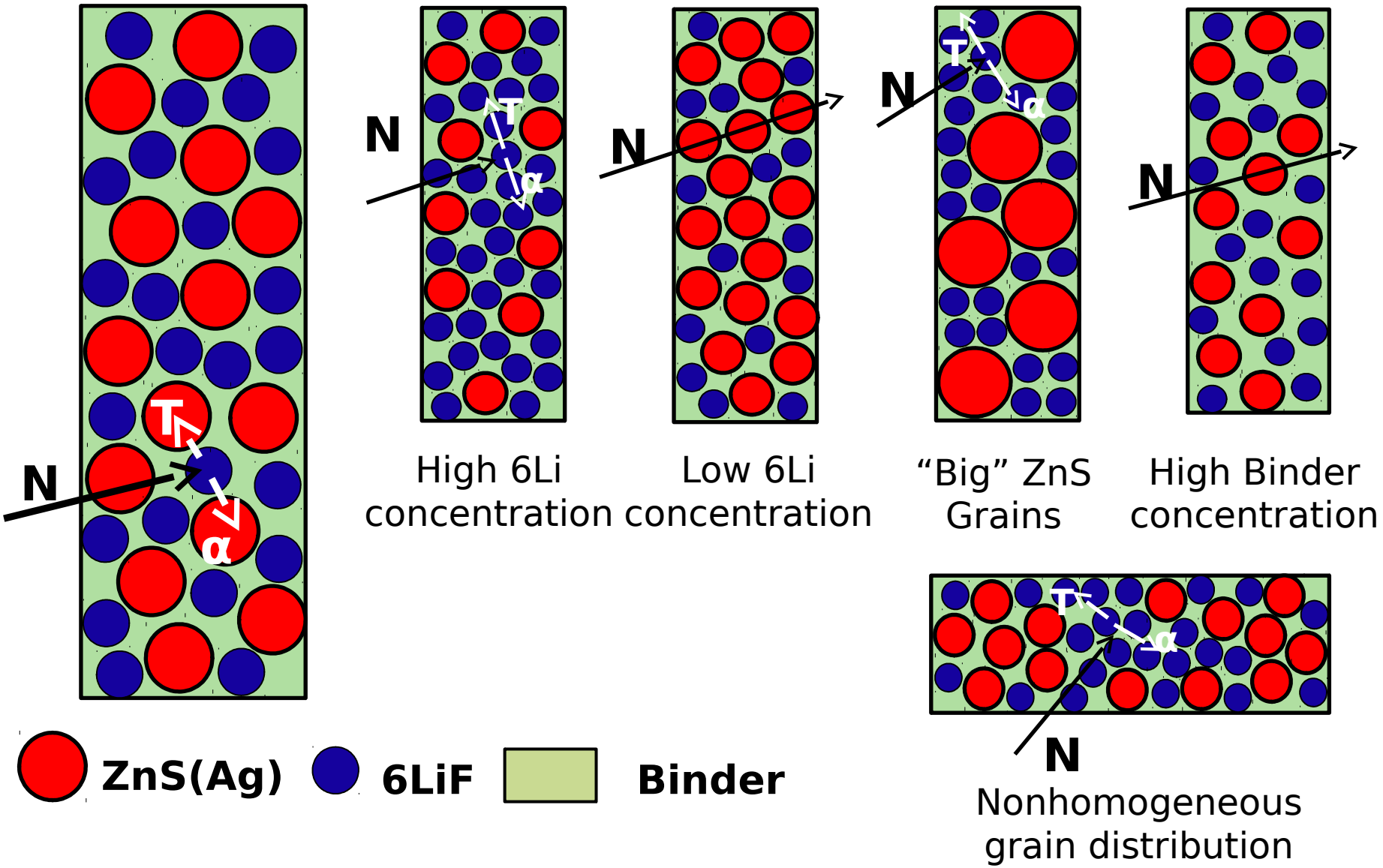

Statistical Analysis of Pulses

Neutron	Gamma	Thermal Noise

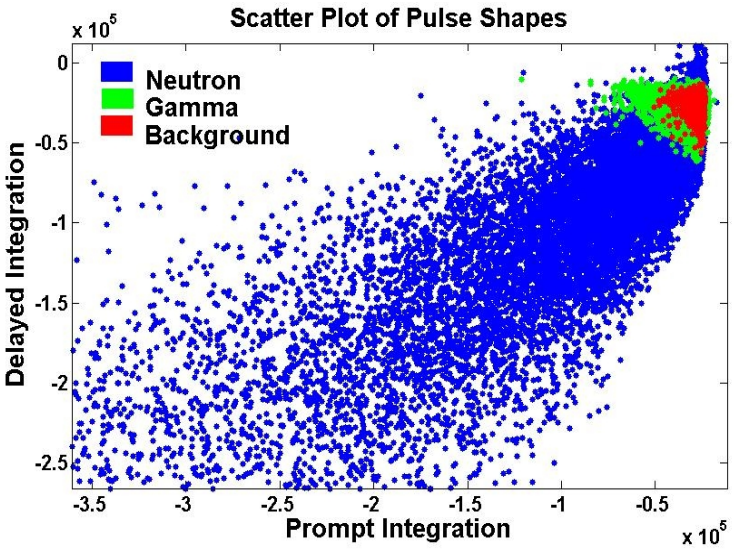

<> Pulse Shape Analysis examines both the pulse amplitude and decay time.

<> Neutrons have a longer scintillation decay time

<> Neutrons are also usually larger in amplitude than gamma events or thermal events.

<> But, there is a large variation in all types of pulses. Thermal events can pile up too.

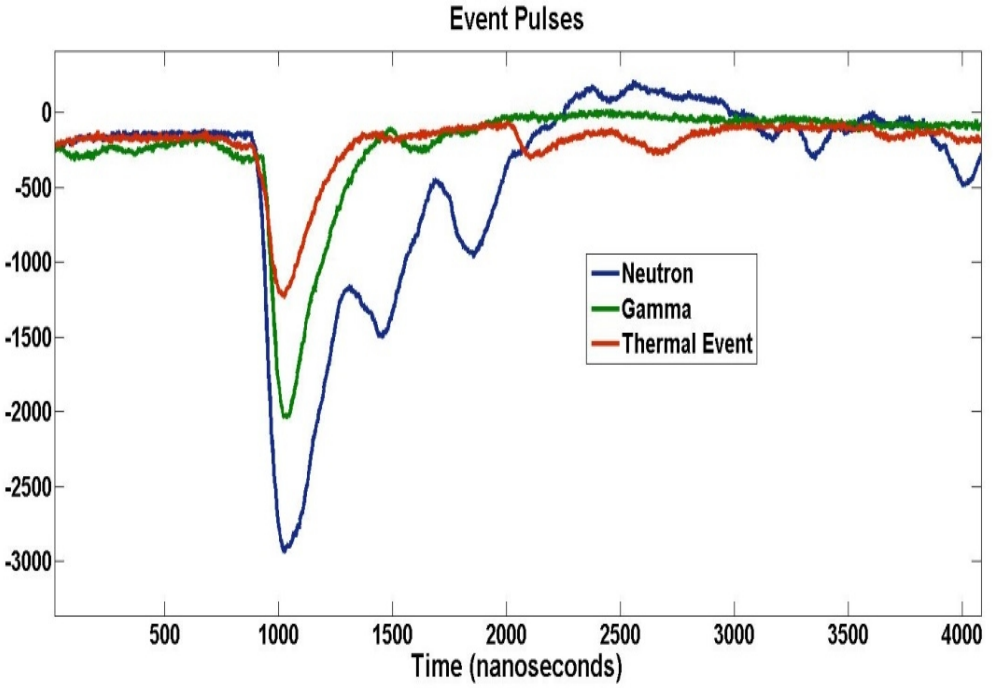

Signal

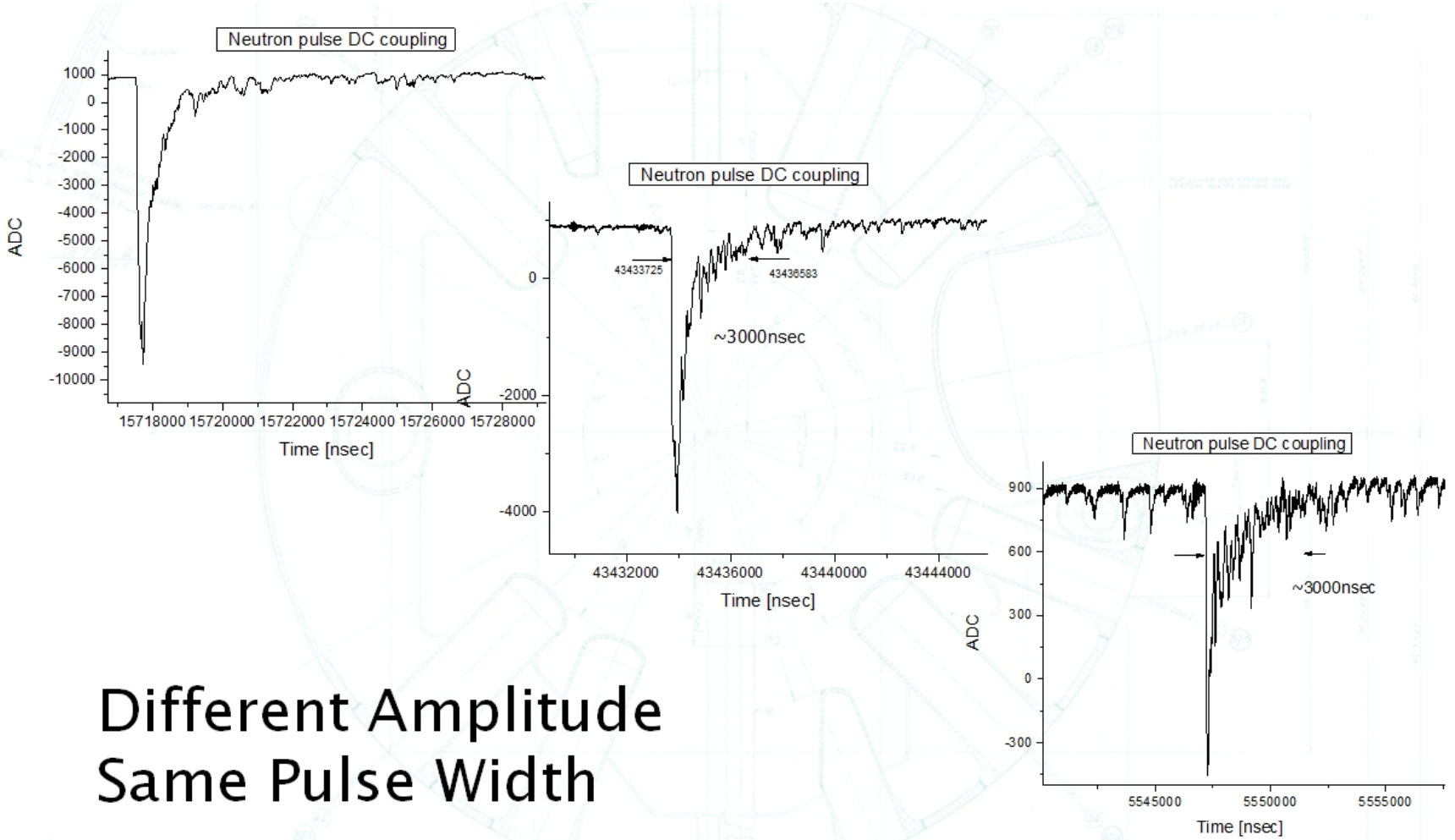

Different Amplitude
Same Pulse Width

SiPM Noise vs. Temperature

- The frequency of thermal noise events increase exponentially with temperature.
- Cooling the diode will give the best SNR result.
- But, a cooling system requirement limits the applications of this detector, and makes the system more complicated.

- Temperature sensors will be used on board with the SiPM to monitor temperature.
- Algorithm parameters can change dynamically to match the temperature conditions.
- Alerts can be sent when the cooling system is underperforming.

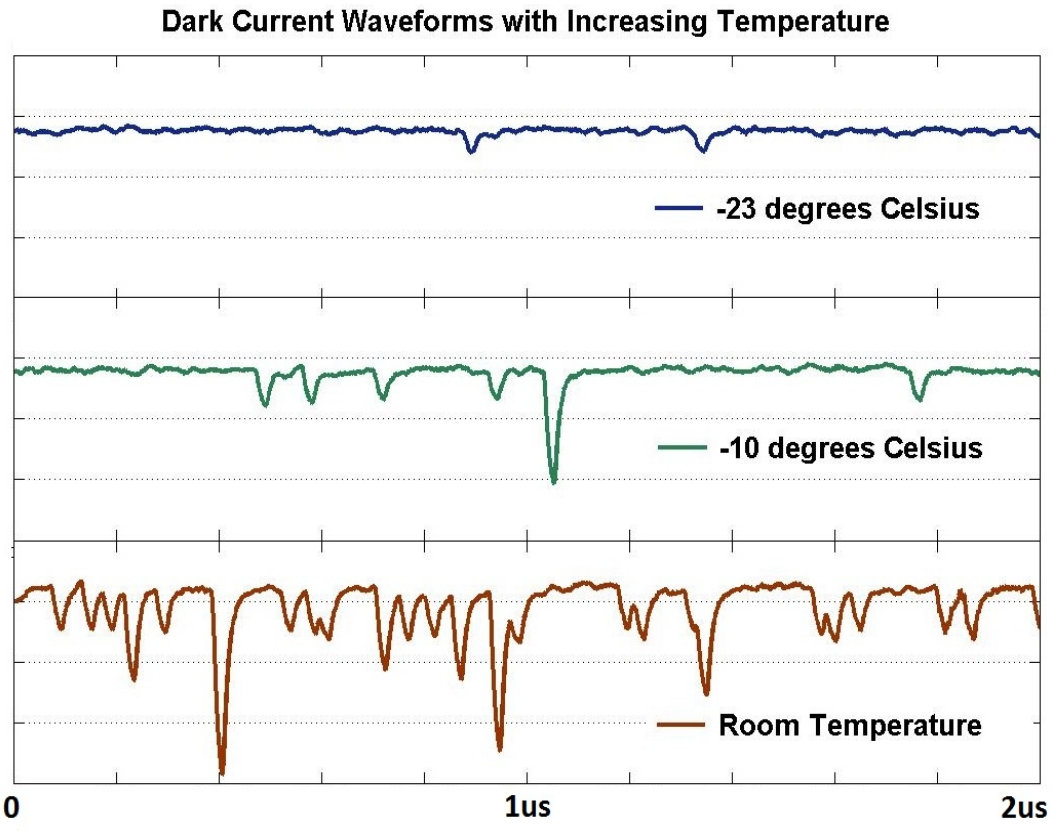

CANDOR Performance and Characteristics

> Typical constant Q resolution, dQ/Q, ~ 0.025

> Fractional wavelength resolution ~ 0.015

> Angular resolution ranging from 1 to 10 minutes (of arc)

> Significantly higher usable intensity incident on sample (possibly an order of magnitude or more increase) without degraded signal-to-noise

Summary – What may be done better with the CANDOR instrument?

> Reach higher wavevector transfer Q and correspondingly improved spatial resolution: as much as 1.5 A-1 (~ half nanometer resolution) at reflectivities as low as 10-9 for single bilayer systems and 3.0 A-1 (~ 2 Angstrom resolution) for a sufficiently ordered multilayer -- assuming background is sufficiently minimized in either case.

> Perform specular reflectivity and diffraction measurements on a given sample much more efficiently, perhaps as much as 100 times faster.

> Realize significantly higher throughput and smaller sample volumes (areas).

> Enable more real time reflectivity measurements and, possibly, direct inversion.

Appendices

Mosaic Crystal (or Multilayer) Analyser Array

> 4 to 6 A wavelength range:

- Pyrolytic Graphite (PG) (002) with 0.5 degree mosaic (FWHM) and peak reflectivity ~ 0.9
- 6 discrete, specularly reflected beams from sample
- 54 crystals and corresponding detectors (1 cm diameter 3He tubes) for each of the 6 channels; 324 separate analyser crystals altogether

> 6 to 10 A wavelength range:

- Ni/Ti multilayer (ML) with ~ 60. A bilayer spacing and ~ 0.8 peak reflectivity
- fluorinated mica with d-spacing of 9.963 A
- NiTi2 thin film crystals – stable metallic compound with strong (111) reflection and interplanar spacing of 5.7735 Angstrom (almost twice that of PG (002) -- thanks to Judy Stalick for this suggestion!)

PG Analyser Array

> if successive PG analysr crystals are each incremented in angle by 1 degree (2 x mosaic FWHM), then negligible wavelength overlap occurs but as many as about half the usable neutrons would be lost

> at a wavelength (WL) of 4.75 A, for example, dWL/WL would be ~ 0.0175

> if the wavelength selection range of successive crystals is *made* to overlap, then the relative probabilities of reflecting neutrons of different wavelengths within this range must be determined (using monochromatic calibration beams and by varying collimation, e.g., defined by a pair of aperture widths, between crystal and corresponding detector, since scattering angle differs with wavelength)

> at 4 A, Bragg angle is ~ 36 degrees, at 6 A ~ 63 degrees

> between 4 and 6 A and for a *sample* reflection angle between 0 and 1 degree, the range of Q covered is approximately 0.055 A-1

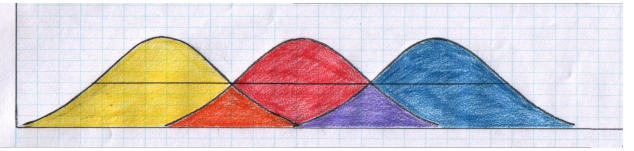

Received internal NIST funding within the “Innovation in Measurement Science” program

ENERGY DISPERSIVE NEUTRON DETECTORS *for* STEADY-STATE SOURCES

Chuck Majkrzak, Jeff Ziegler, Nick Maliszewskyj, and Richard Ibberson
NIST Center for Neutron Research

NIST
National Institute of Standards and Technology
U.S. Department of Commerce

Physica B 173 (1991) 75–88
North-Holland

Invited paper

Polarized neutron reflectometry

C.F. Majkrzak
National Institute of Standards and Technology, Gaithersburg, MD 20899, USA

Polarized neutron reflectometry is a powerful technique for studying the microscopic magnetic structures in thin films and multilayers. The corresponding analysis of spin-dependent reflectivity data is discussed and illustrated with a number of specific examples. The measurement of the precession of the neutron moment within a nonmagnetic medium, but in the presence of an applied field, as a means of determining the nuclear density profile is also considered.

1. Introduction

It is widely known that neutron diffraction is the single most important method of determining the microscopic magnetic structures of bulk solids. It has been further demonstrated that the sensitivity afforded by the dipolar coupling between neutron and atomic magnetic moments can be, in certain cases, appreciably enhanced if the neutron polarization before and after scattering is measured. Given the magnitudes and orientations of the atomic moments as a function of temperature or field by this method, fundamental physical properties of the system, such as its critical behavior, can be deduced.

Despite the relatively small amount of material contained in thin films or multilayer samples, significant information regarding the magnetization profile normal to the surface can also be obtained by neutron reflection, both about the forward scattering direction and at higher momentum transfers if the sample is crystalline. The purpose of this paper is to illustrate how such data are obtained and analyzed. First, the reflectometer itself is described, that is, how the incident beam is polarized and the neutron spin state flipped, what the instrumental resolution and flux at the sample are, and so on. Next, the kinematical and dynamical theories of diffraction or reflection are discussed for polarized beams, in regard to the analysis of the reflectivity data, and illustrated with a number of specific examples. Finally, the possibility of using the precession of the neutron moment in an applied field within nonmagnetic material to extract the nuclear scattering density profile is discussed. The novel technique of grazing angle diffraction, which has just recently been demonstrated for polarized neutrons, is described in a separate paper by Ankner et al. [1].

2. Instrument

In this section a polarized neutron reflectometer located on beam tube BT-7 at the Neutron Beam Split-core Reactor (NBSR) at the National Institute of Standards and Technology (NIST) is described. This reflectometer utilizes a continuous, nearly monochromatic and highly parallel beam of polarized neutrons incident on the sample. Polarized neutron time-of-flight (TOF) reflectometers also exist but will not be described here (see, for example, ref. [2] for a description of such a machine).

In fig. 1 is shown a schematic of the reflectometer. The polychromatic beam first passes through a pyrolytic graphite (PG) filter to suppress the higher order wavelengths which would also be reflected by the vertically focussing PG monochromator set for a principal wavelength λ of 2.35 Å. For collimations of the order of one degree and one minute of arc preceding and following the monochromator, respectively, the

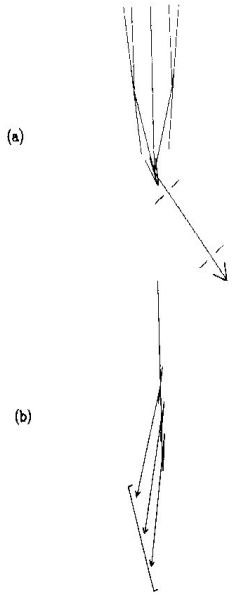

Fig. 3. (a) Schematic showing how a convergent section of supermirror guide can be used in conjunction with a multiple piece graphite monochromator to increase the wavelength spread of the incident beam in a reflectometer; (b) a specularly reflected polychromatic beam incident on a series of multilayer monochromators of different spacings and/or angles, each set to reflect a particular band of wavelengths onto a different section of a position sensitive detector as discussed in the text (from ref. [5]).

3. Data analysis

The neutron reflectivity of a film or multilayer can be measured from small values of Q about the forward scattering direction out to higher values of Q about positions corresponding to atomic plane periodicities in single crystalline superlattice films. At the lower values of Q where the reflectivities can approach unity, a dynamical theory is required, whereas at higher Q, where the reflectivity is often far from unity and extinction of the incident beam is negligible, a simpler kinematical treatment suffices.

3.1. Kinematical analysis

In the kinematical diffraction limit the squares of four structure factors F can in principle be measured corresponding to spin-flip (SF) and non-spin-flip (NSF) scattering processes [7]. When utilizing a polarized incident beam and analyzing the polarization state of the reflected beam, one particularly useful configuration is that in which the polarization axis $\boldsymbol{P}$ is parallel to the applied field $\boldsymbol{H}$ and perpendicular to $\boldsymbol{Q}$ as shown in fig. 4 where $\hat{S}_j$ is a unit vector in the direction of the net magnetic moment in the reflecting plane at an angle ϕ_j relative to $\boldsymbol{H}$. For an epitaxially grown single crystal superlattice, if b_j and p_j are the average nuclear and magnetic scattering lengths for the jth atomic plane and u_j the position of that plane along an axis parallel to $\boldsymbol{Q}$, then (assuming for simplicity that the atomic densities are the same for all planes) [8]

$$F^{\pm\pm} = \sum_j (b_j \mp p_j \cos\phi_j)\, e^{iQu_j}, \tag{2}$$

and

$$F^{\pm\mp} = \sum_j p_j \sin\phi_j\, e^{iQu_j} \tag{3}$$

where the superscripts refer to the initial and final neutron spin eigenstates and $\boldsymbol{Q}$ is normal to the substrate surface. The magnetic form factor is included in p_j and is in general Q-dependent. Thus, in this particular arrangement, the component of the magnetization parallel to the applied field $\boldsymbol{H}$ gives rise to non-spin-flip scattering, which interferes with the nuclear scattering,

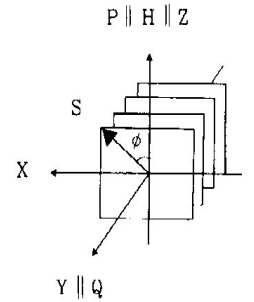

Fig. 4. Polarized beam reflection geometry for multilayers referred to in the text.

A comprehensive study was undertaken to determine whether or not a beam modulation method would be a suitable alternative for a polychromatic reflectometer. It was concluded that insofar as measurements of the specular reflectivity are concerned, modulation techniques can yield, at best, a given statistical accuracy with an efficiency no better than that achieved with a single monochromatic beam having comparable instrumental resolution. However, a polychromatic incident beam with wavelength analysis of the reflected beam performed directly by physical devices, e.g., crystal analyzers, is significantly more efficient.

Langmuir **2009,** *25,* 4145–4153

Analysis of Multibeam Data for Neutron Reflectivity[†]

N. F. Berk*[,‡,§] and C. F. Majkrzak[§]

Department of Materials Science and Engineering, University of Maryland, and NIST Center for Neutron Research, National Institute of Standards and Technology, 100 Bureau Drive, Stop 6102, Gaithersburg, MD 20899-6102

Received August 26, 2008. Revised Manuscript Received December 3, 2008

We offer mathematical proof that multiple-beam neutron reflectivity, corresponding to simultaneous collection of data at multiple angles (wavevector transfers) does not perform better, errorwise for counting noise, than single-beam data collection for the same total number of reflected neutrons—and may perform much worse, depending on the beam modulation strategy used. The basic idea is that the nominal statistical benefit of summing data at, say, N different wavevector transfers is undone by needing to collect N differently modulated (i.e., weighted) sums in order to extract the reflectivities. To our knowledge, a general proof of this behavior for arbitrary strategies has been lacking. The formal result can be summarized by saying that the best nondiagonal matrix modulation strategies are orthogonal (unitary) matrices, or constant multiples thereof, and that these can do no better than diagonal—i.e., single-beam—strategies.

Introduction

We offer mathematical proof that multiple-beam (or "multiplexed") neutron reflectivity, corresponding to simultaneous collection of data at multiple angles (wavevector transfers) does not perform better, errorwise for counting (shot) noise, than single-beam data collection for the same total number of reflected neutrons—and may perform much worse, depending on the beam modulation strategy used. The basic idea is that the nominal statistical benefit of summing data at, say, N different wavevector transfers is undone by needing to collect N differently modulated (i.e., weighted) sums in order to extract the reflectivities. Such behavior has been described before,[1] but to our knowledge a general proof for arbitrary strategies has been lacking. The formal result can be summarized by saying that the best nondiagonal matrix modulation strategies are orthogonal (unitary) matrices, or constant multiples thereof, and that these can do no better than diagonal—i.e., single-beam—strategies.

In this paper we lay out precisely what we mean by multiple-beam measurements and discuss shot noise "error" propagation through such systems. We derive a multiplication factor for the average weight of observed reflectivity noise relative to the average weight of the associated single-beam reflectivity noise and prove a theorem that this factor cannot be less than unity for any beam modulation strategy. The smallest possible value, unity, of the noise factor is achieved only by "trivial" (diagonal matrix) strategies and by nontrivial modulations described by orthogonal (unitary) matrices. Ill-chosen (nonunitary) strategies can lead to noise that grows with the number of beams in the configuration, as we illustrate in the Examples section. In the Conclusions, we briefly comment on recent innovative uses of divergent beams (a form of multiplexing) in reflectivity studies.[2,3]

[†] Part of the Neutron Reflectivity special issue.

* Corresponding author. E-mail: nberk@nist.gov.

[‡] University of Maryland.

[§] NIST.

(1) Harwit, M.; Sloane, N. J. *Hadamard Transform Optics*; Academic Press: New York, 1979. These authers show that other error types can benefit from multibeam strategies.

(2) Rekveldt, M. Th.; Bouman, W. G.; Kraan, W. H.; Uca, O.; Grigoriev, S. V.; Habicht, K.; Keller, T. Elastic Neutron Scattering Measurements Using Larmor Precession of Polarized Neutrons. In *Lecture Notes in Physics, Neutron Spin Echo Spectroscopy, Basics, Trends, and Applications*; Mezei, F., Gutberlet, T., Pappas, C., Eds.; Springer: Berlin, 2003; p 87.

Inverting Multiple Beam Data

Noiseless Data. Consider an instrument consisting of N beams simultaneously incident on a reflecting film. These beams have known intensities, B_n, $n = 1,..., N$, comprising the set denoted by $\{B_n\}_N$. The corresponding reflected beams are detected by N detectors configured to correspond to known scattering wavevectors $\{Q_s\}_N$, $s = 1,..., N$ at known wavelengths. We label each such reflected beam by the index s, for "slot." In the absence of counting noise, the ideal reflected intensities comprise the set $\{I_s\}_N$, where $I_s = B_sR_{0s}$, and where $\{R_{0s}\}_N$ are the theoretical reflectivities associated with the corresponding $\{Q_s\}_N$ (the "0" subscript denotes their theoretical nature). Thus each slot also is associated with a "perfect" reflectivity, $R_{0s} = R_0(Q_s)$. For specular reflection, each detector records only a single reflected signal—viz., the I_s "in" slot s—and there is no problem in identifying the unique reflectivities $R_{0s} = I_s/B_s$ in each slot. For nonspecular reflection, however, a given detector may receive up to N reflected beams, corresponding to all the $\{Q_s\}_N$ in the configuration. The resulting signal in the *given* detector thus is the sum of signals

$$S = \sum_{s=1}^{N} I_s = \sum_{s=1}^{N} B_s R_{0s} \tag{1}$$

(Of course, some R_{0s} may be zero in the given detector.) Clearly, a single measurement of S is insufficient to determine $\{R_{0s}\}_N$ uniquely, even though $\{B_n\}_N$ is known. However, by performing N separate measurements, $S_1, S_2,..., S_N$, in the same detector, with each one corresponding to different sets of incident beams over the N slots, $\{B_{1s}\}_N, \{B_{2s}\}_N,..., \{B_{Ns}\}_N$, we obtain the set of equations

$$S_m = \sum_{s=1}^{N} I_{ms} = \sum_{s=1}^{N} B_{ms} R_{0s} \tag{2}$$

for $m = 1,..., N$. Here we we use index m for "measurement." In obvious matrix notation, these measurements are summarized as

$$S = BR_0 \tag{3}$$

where S and R_0 are N-dimensional column vectors and B (sometimes notated below as B_N) is an $N \times N$ matrix consisting of N rows (the mth row representing a measurement S_m) and N

10.1021/la802780v CCC: $40.75
Published on Web 01/30/2009

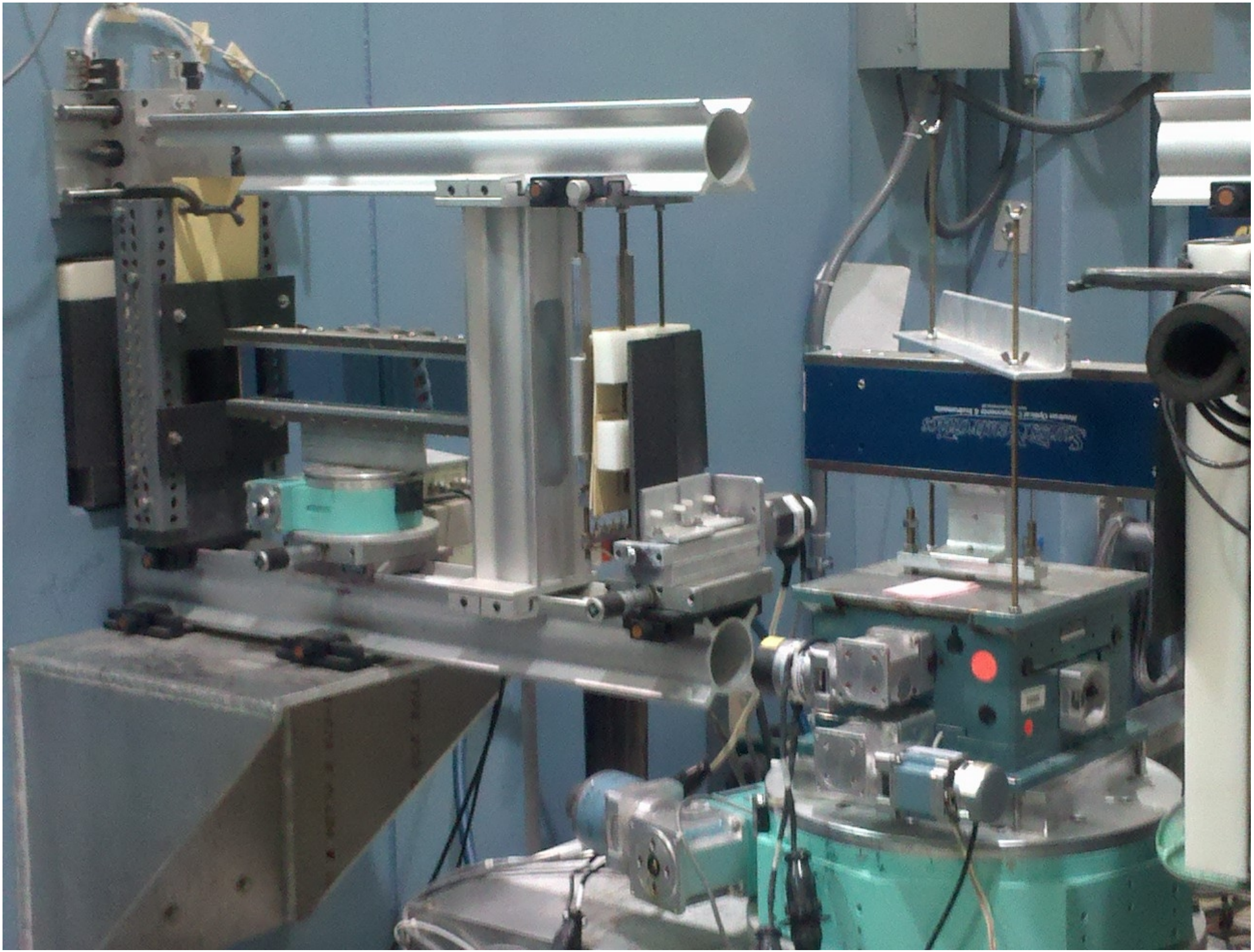

Polarizing V-Cavity

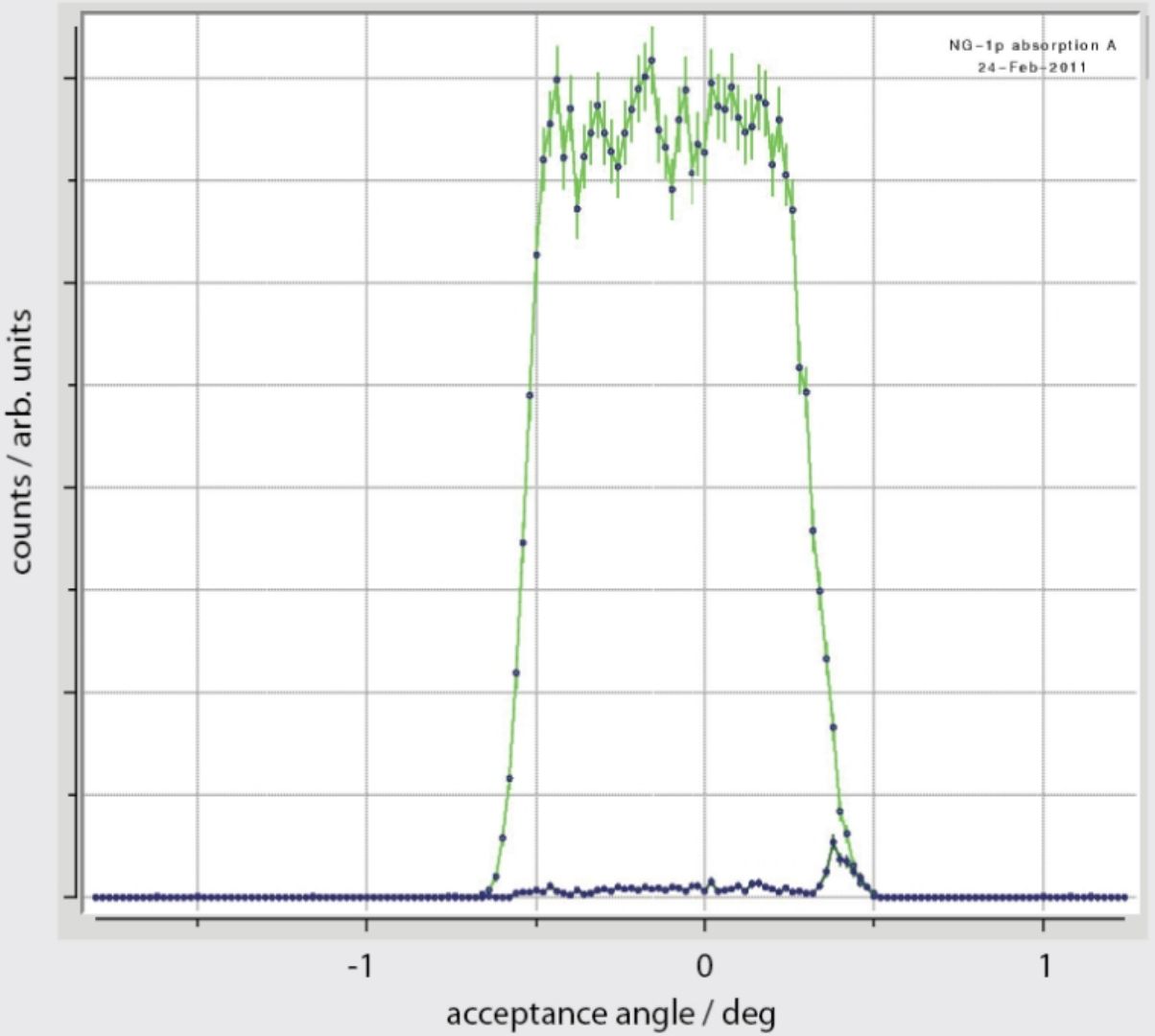

Test measurement of a prototype test piece. The transmission of the desired spin state at 4.75 Å was 84% and the polarizing efficiency was 98%.

Left: Test measurement of a prototype Swiss Neutronics polarizing V-cavity. The desired spin state (green line) is transmitted within the acceptance angle range, and the alternate spin state (blue) is rejected.

6LiF:ZnS(Ag) - Detection Process

- **Diffracted neutrons are captured by 6Li in the scintillator (6Li (n,α) 3H).**
- **When the neutron is absorbed a 2.06 MeV alpha particle and a 2.74 MeV triton are ejected in opposite directions.**
- **The alpha particles and tritons can travel only for a few microns in the scintillation compound (α ~ 0.007mm, T ~ 0.04mm).**
- **While traveling, the alpha particles and tritons lose energy and ionize the scintillation compound.**

Test Setup -- 4.75 A Neutrons

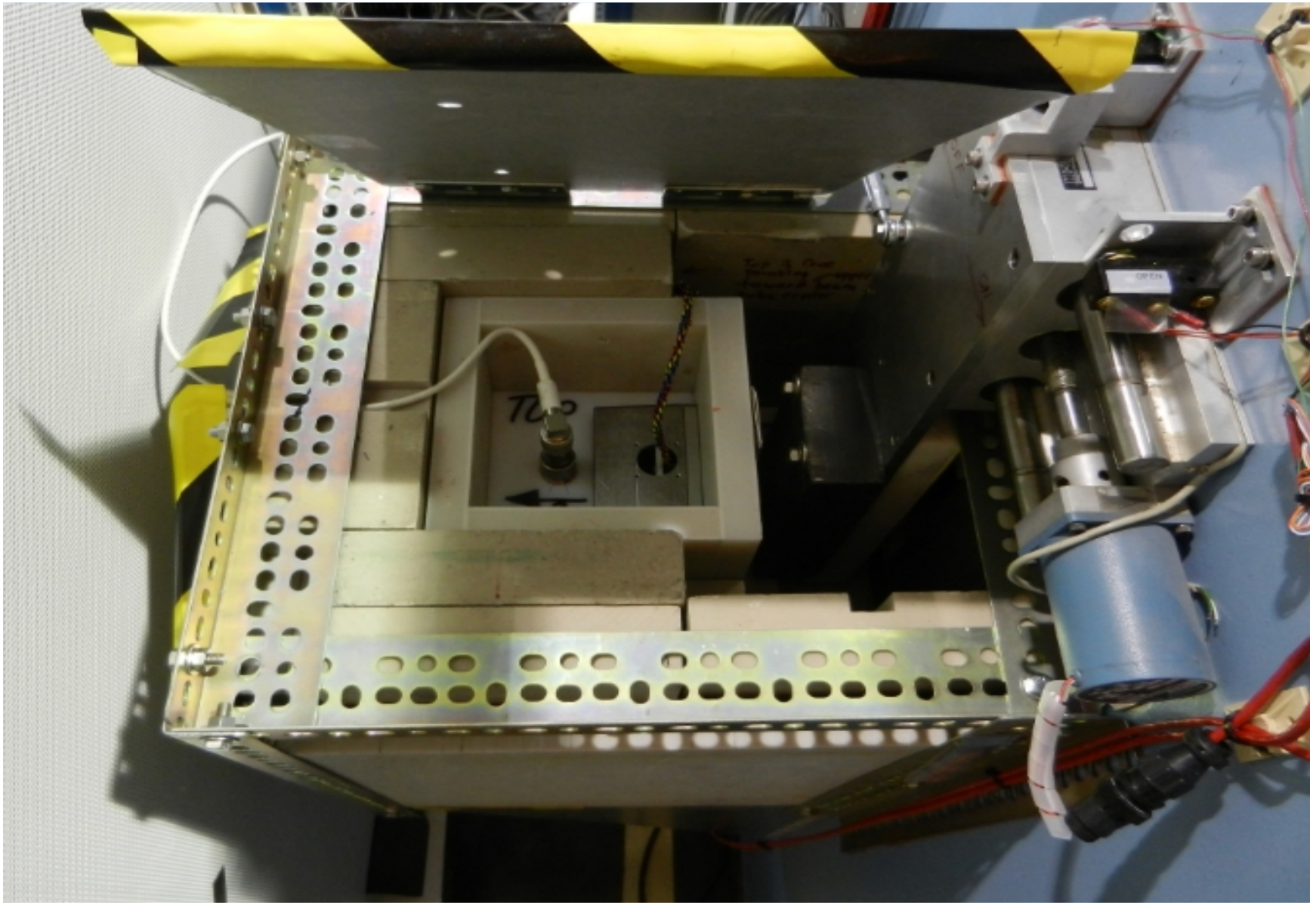

Gamma Events

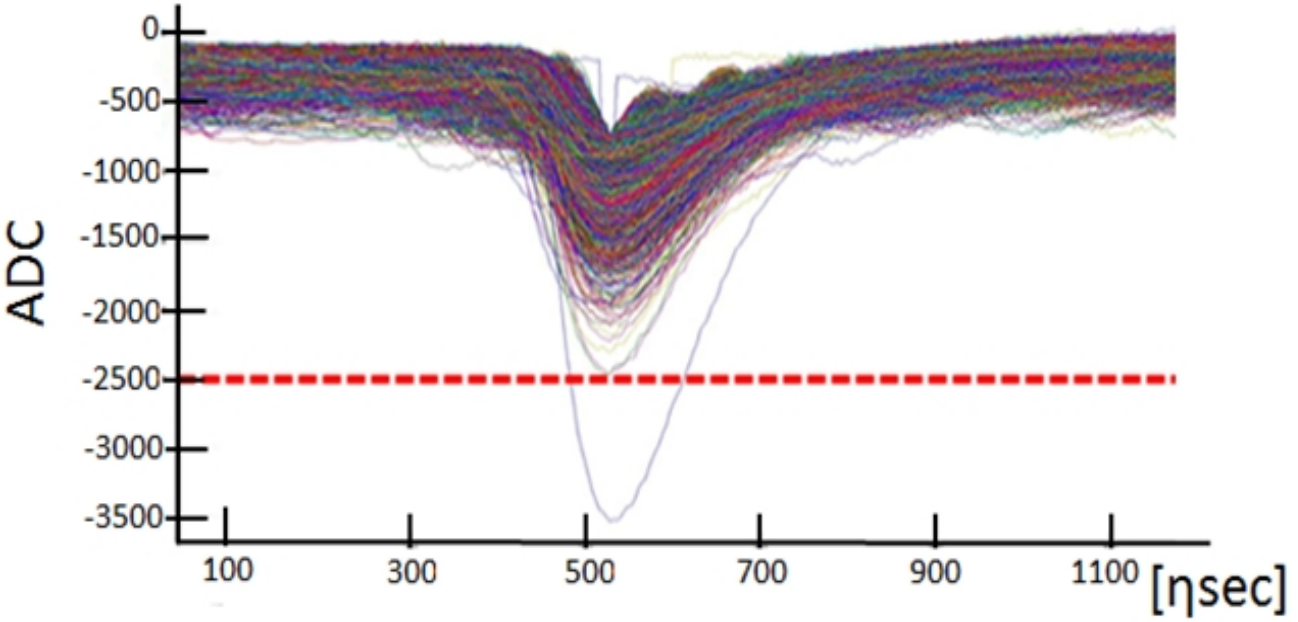

Neutron Events

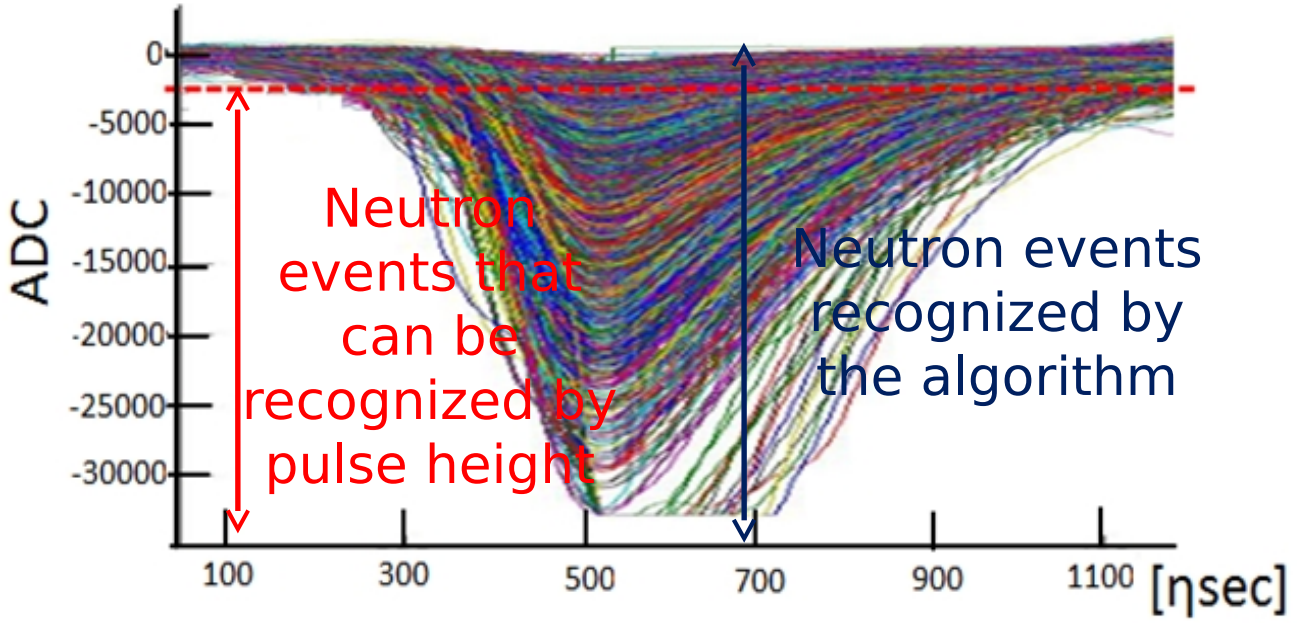

Gamma Rejection

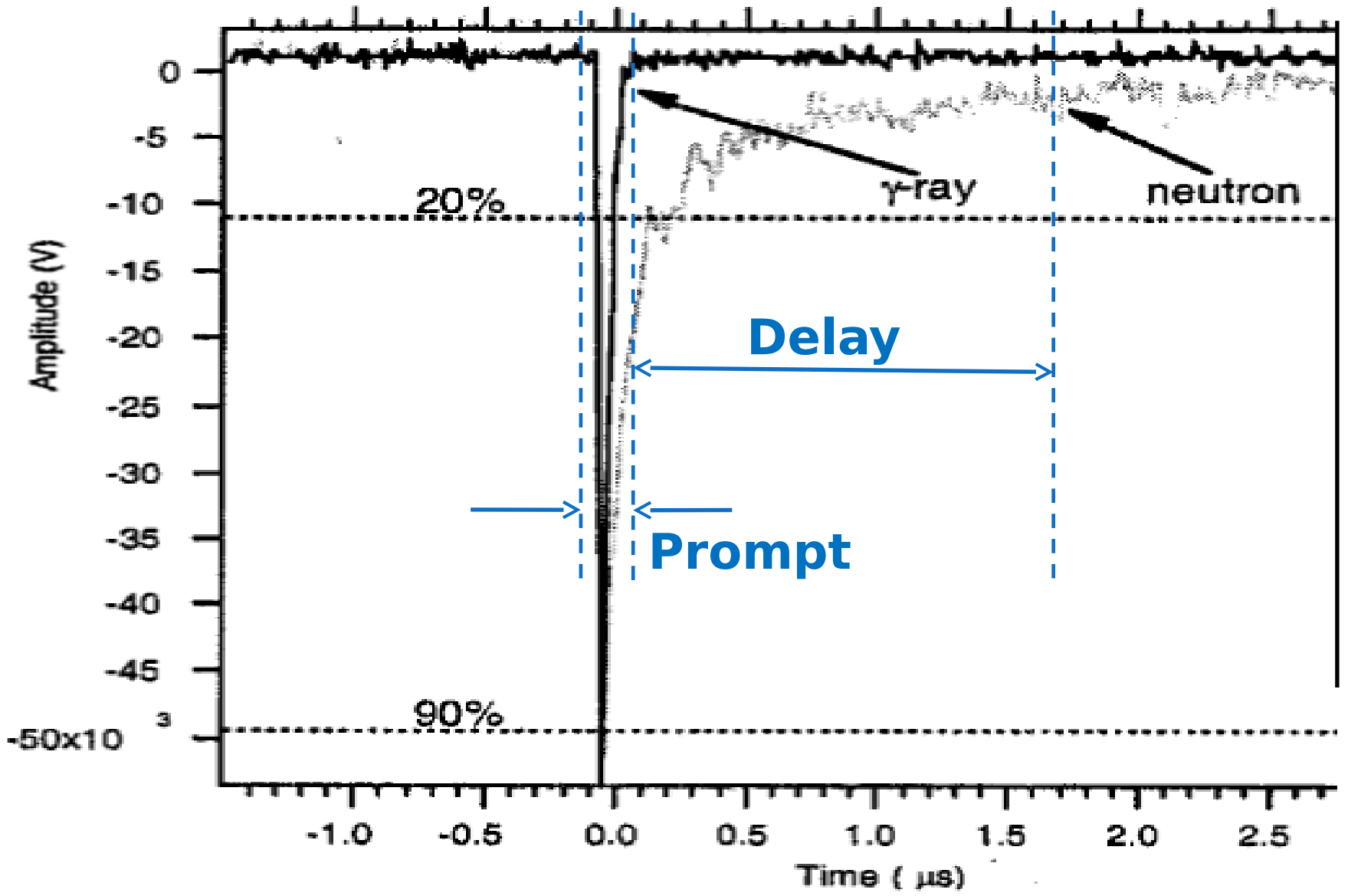

Jeff Sykora http://neutrons.ornl.gov/conf/insis2012/presentations/Scintillators_Sykora.pdf

Neutron Sensitivity

Configuration	Rate [cps]	Result
Helium Tube Detector	1140	
CANDOR prototype detector (Helium detector 128 cps)	1012	Stopping power: 90%
CANDOR real time discriminator	523	Detection efficiency: 46%

Gamma Sensitivity

Configuration	Incident photons	Measured Photons	Gamma Rejection
Cobalt-60	3.9x10^8	87 counts	1 per 0.44x10^7
Cesium-137	1.5x10^8	5 counts	1 per 6.6x10^7
Back ground	Less than 1count per 10 min. measured for about 1 hour		